

A general model for comprehensive electrical characterization of photovoltaics under partial shaded conditions

Fuxiang Li^a, Wentao Dong^b, Wei Wu^{a,*}

^a School of Energy and Environment, City University of Hong Kong, Hong Kong, China

^b Department of Computer Science, City University of Hong Kong, Hong Kong, China



ARTICLE INFO

Keywords:

Photovoltaic
Partial shading condition
Equivalent circuit
Current mismatch
Reverse biased

ABSTRACT

Partial shading condition (PSC) causes underperformance, unreliability, and fire risks in photovoltaic (PV) systems. Accurate estimation of PV behaviors is crucial to fundamental understanding and further mitigation. However, current modeling methods lack full consideration of the physical behaviors, system complexities, and shading pattern diversities, ending in coarse and simple analysis. Herein, an innovative modeling approach with high-performance algorithms is proposed to address these challenges simultaneously. Based on rigorous analysis, physics models considering the reverse-biased behaviors, the system complexities, and shading pattern diversities, are developed at the cell, module, and array levels, respectively. Then, a strict and progressive validation via measurement data is conducted to justify the effectiveness of the developed method. The method is valid for mainstream PV technologies in the market and can predict cell behaviors and module electrical characteristics perfectly. Notably, the proposed method is more computationally efficient than Simulink when simulating the same PV array. Lastly, to demonstrate its exclusive advantages, two case studies are conducted. The localized power dissipation can be quantified. The observed energy loss justifies the necessity of reverse biased behaviors and high-resolution simulation. This method can be coded in any development environment, providing an efficient and comprehensive tool to analyze PV systems.

1. Introduction

1.1. Motivation and challenges

The surging frequency of extreme weather and the deteriorating environment alerts the world to curb CO₂ emissions by reducing the reliance on fossil fuels and moving toward renewable energy [1,2]. Due to the low carbon footprint, technological maturity, and low barrier of entry, photovoltaics (PV) represents a promising alternative to address the global energy dilemma [3,4]. Revent years have witnessed a surging popularity of adopting PV in near-net zero energy buildings [5,6], microgrids [7], power generation systems [8]. High power conversion efficiency (PCE) with long-term stability is the eternal pursuit and key challenge of PV research and development (R&D). Despite the breakthroughs that have been made in the laboratory, the PCE and lifetime in real-world conditions are still far from expected due to the underperformance and unreliability issues [9,10].

Partial shaded condition (PSC), referring to the non-homogeneous irradiance distribution in the PV system, is considered the most frequent and critical cause of this dilemma [11]. Firstly, PSC usually induces a reverse-biased state in the shaded solar cells, leading to the power mis-

match phenomenon and thus causing significant power loss [12]. Worse still, these reverse-biased cells do not serve as power generators, however, they sink power and heat themselves, inducing the degraded PCE and localized heating effect (hot spot), which can permanently damage the PV module and even cause fire hazards [13]. Thirdly, using bypass diodes (BPD) can mitigate this adverse effect but induces a power-voltage (P-V) curve with multiple peaks, usually with a global maximum power point (GMPP) and several local maximum power points (LMPP). Consequently, the maximum power point tracking (MPPT) can be easily cheated at LMPP, which potentially leads to unnecessary yield reduction [14].

Considering its detrimental effects on the efficiency, reliability, as well as safety of PV systems, it is critical to study the behaviors of PV under PSC and propose mitigating measures. Abundant factors from both ambient (irradiance, PSC, temperature, wind speed, etc.) and the PV system itself (technologies, system layout, etc.) are associated with this phenomenon. Experimental studies cannot cover such multi variables and may lead to unbearable costs. Therefore, major research initiatives have been directed to propose a scientific, reasonable, and accurate mathematical model.

1.2. Literature review

Currently, the equivalent circuit method (ECM) is dominant in PV system modeling, due to the ability to reveal the current-voltage char-

* Corresponding author.

E-mail address: weiwu53@cityu.edu.hk (W. Wu).

Nomenclature

<i>a</i>	fraction of current involved in avalanche breakdown
CS	cell string
E_g	band-gap energy for the semiconductor material, eV
G	solar irradiance, W/m ²
I	current, A
K_i	short-circuit current temperature coefficient, mA/K
K_v	open-circuit voltage temperature coefficient, mV/K
k	number of the cell strings in the module
k_B	Boltzmann constant, J/K
MS	module string
m	avalanche breakdown exponent
n	number of the cells in the cell string
N_p	number of solar cells in a module connected in parallel
N_s	number of solar cells in a module connected in series
q	electron charge, 1.60217646·10 ⁻¹⁹ C
R	electrical resistance, Ω
T	temperature, °C
\mathbf{T}^M	temperature matrix of the module
\mathbf{T}^A	generalized temperature matrix of the array
t	elapsed time, s
u	wind velocity, m/s
V	voltage, V

Greek symbols

ϵ	absolute errors
γ	ideality factor of the diode
σ	Stefan-Boltzmann constant, W/(m ² ·K ⁴)
Ω^M	shading matrix of the module
Ω^A	generalized shading matrix of the array
ω	shading factor

Superscripts

a	array
BLD	blocking diode
BPD	bypass diode
c	cell
m	module
ms	module string

Subscripts

o	reverse saturation
amb	ambient
br	junction breakdown
d	diode
ex	extraction
gro	ground
i	the number of the iteration
j	j th cell in the cell string
oc	open circuit
p	parallel resistance
ph	photocurrent
s	series
sc	short circuit
t	thermal
v	voltage

Abbreviation

ANN	Artificial neural networks
BIPV	Building integrated with photovoltaic
BPD	Bypass diode
BLD	blocking diode
DDM	Double-diode model
ECM	Equivalent circuit method

GC	General condition
GMPP	Global maximum power point
GPR	Gaussian process regression
LMPP	Local maximum power point
MDM	Multi-diode model
MPPT	Maximum power point tracking
NOCT	Nominal operating cell temperature
NRM	Newton-Raphson method
PCE	Power conversion efficiency
PSC	Partial shaded conditions
PV	Photovoltaic
R&D	Research and development
SDM	Singe-diode model
SP	Series-parallel
SSDM	Segmented singe-diode model
STC	Standard testing condition
SVM	Support vector machine
UIC	Uniform irradiance condition
STC	Standard test condition

acteristics (I-V curve) [15]. ECM has been widely used to study the PV system under uniform irradiance conditions (UIC). Examples includes the single-diode model (SDM) [16], double-diode model (DDM) [17], and multi-diode model (MDM) [18], etc. By including the effects of shadows in these elementary models, ECM can be utilized in modeling the PV under PSC. Thus, the following literature review mainly focuses on the state-of-the-art and challenges in this field.

1.2.1. State-of-the-art

Different from the UIC, there are multiple irradiance levels on the PV under PSC. To characterize the PV performance, a natural idea is to integrate the non-uniform irradiances into the ECM used for UIC. A DDM with an improved iteration method was proposed by Kermadi et al. [19]. The model was solved in MATLAB to obtain the electrical characteristics of the PV array. However, the method is based on the assumption that there is uniform irradiance on the module. Using several assumptions, Bai et al. [20] developed an SDM with an iteration-free method. The method was complete, and the efficiency was high, however, a notable deviation could be found in the experimental validation, especially near MPP. Furtherly, Zhu et al. [21] developed a similar model to predict the power output of the building-integrated PV (BIPV). The shading effect on the single cell's parameter was discussed detailly and the effectiveness of this method was validated by a module-level experiment. Ma et al. [22] proposed an analytical method assisted by a novel shading information extraction method to simulate the performance of PV strings under PSC. A four-state Jaya algorithm was particularly implemented in the parameter extraction process to improve the accuracy. Wu et al. [23] specialty developed a complete method to evaluate the performance of a semi-transparent photovoltaic glazing façade. In their experiment validation, the method worked well in the UIC scenarios, but a large deviation was observed when simulating the electrical behaviors of the façade under small-scale PSC. Generally, these studies provided valuable tools to improve our understanding of PV under PSC. Unfortunately, the observed deviations indicate that directly integrating the non-uniform irradiance into the ECM for UIC is not the optimal choice for accurate modeling of PSC.

To overcome these shortcomings, the in-depth effect of PSC on the PV behaviors should be considered: when PSC occurs, shaded cells stop generating power gradually and begin to dissipate the power generated from the non-shaded cells. This phenomenon is known as reverse-biased effects and is recognized as the root cause of power loss and other negative effects [24]. In the 1980s, Bishop [25] conducted fundamental studies of reversed-biased solar cells, which laid a solid basis for subsequent research. Using a similar approach, Gutierrez et al. [26] pro-

posed a method to estimate the electrical performance of large PV arrays including the reverse-biased cells. The results highlighted the significance of using the bypass diodes to mitigate the power loss under PSC. Zhang et al. [27] combined the traditional SDM with the Bishop method to develop a hybrid model. An explicit expression of the I-V curve was derived, and the effectiveness of the proposed method was fully demonstrated via experimental validation. Besides electrical performance characterization, consideration of reverse-biased effect also allows an in-depth understanding of the mechanisms of some faults, which could greatly facilitate the R&D of mitigation measures. For example, using an SDM considering reverse-biased behaviors, Zhang et al. [28] developed a diagnosis method for PV modules with hot spots and cracked cells. The method showed high sensitivity to small mismatches and had significant practical application values. As indicated, full consideration of the reverse-biased effect contributes to a comprehensive, in-depth understanding and accurate estimation of the electrical behaviors of PV under PSC, which is beneficial to the enhancement of both power output and lifespan.

1.2.2. Challenges in applications

Despite the mentioned advantages, the existing methods are either specific methods for given conditions or pure theoretical analysis, which show limited applicable values and end in coarse analysis. As a result, they cannot address the real needs in both engineering and research. To bridge this gap, the complexities and needs of real-world engineering should be carefully analyzed and then addressed in an innovative model.

Firstly, the diversity of PV technologies and system topologies should be considered. There are multiple available technologies and system topologies for PV systems. When PSC occurs, the seriousness of the adverse effects is highly associated with the two aspects. On one hand, different PV technologies under the same PSC pattern may have totally different electrical characteristics [29]. To minimize the loss, the PV cell technology should be evaluated and selected properly in the stage of project planning. This requires the modeling method should be generalized enough to be applied to mainstream PV technologies. On the other hand, the system layout could be optimized to diminish the adverse effect of PSC. In the PV module, the length of the cell string can be optimized to reduce the susceptibility to the PSC [29]. Recently, half-cut cell design [30] and shingled modules [31,32] are also popular choices in the engineering field to achieve the same goal. Moreover, array topology reconfiguration, featuring the modification of PV module interconnections and hardware implementation, has attracted surging research interest recently [33,34]. Regardless of the kind of reconfiguration techniques, modeling the electrical characteristics is the first and decisive step [35]. Yang et al. systematically reviewed the existing reconfiguration techniques and compared their performance in applications [36,37]. Existing methods were either applicable to certain types of PV systems or simplified analysis of real-world shading diversities. Meanwhile, they found that unreliable modeling results can degrade the reliability of the MPPT algorithms based on the exploitation of I-V curves [38]. As indicated, in engineering practice, mitigating the adverse effect of the PSC needs efforts on different levels (cell, module, and array). Simultaneously, the emerging research in enhancing PV performance under PSC requires that the electrical characteristics must be calculated in a multiscale way. However, most existing studies are specified methods for one scale, lacking the full consideration of the diversities of the PV technologies and system topologies.

Secondly, the diversity of the shading patterns should be considered. Currently, the PV system has received increasing popularity in applications and has been exposed to various shading patterns inevitably. In the urban context, the rooftop or BIPV systems are usually adapted to their deployed sites and thus exposed to the shadows from the surroundings. There have been several studies to use machine learning to assist such project planning or performance projection, but few of them consider the building shadows [39]. Different building morphologies and neighboring can lead to complex shading patterns, potentially causing

high energy losses and fire risks [21,40]. In a large PV power plant, due to the large surface area, the moving clouds can easily cause PSC and leads to rapid power fluctuations, which greatly challenge the grid transient stability [41]. Besides, multiple factors from ambient, such as accumulated soiling, bird droppings, fallen leaves, etc., can also lead to PSC [42]. Despite their small scales, significant power loss and hot spots can be caused in the shaded module as PV cells are interconnected in the module [43]. In general, PSC can occur in a broad range: from a very small area to a large area, and usually are uneven. Thus, reliable PV modeling must consider the PSC patterns at least on the cell level. Unfortunately, this point is rarely reported on the PV array level.

Lastly, the simulation efficiency should be considered. On top of the high accuracy, improving computational efficiency is also significant, especially in large systems [44]. Since ECM is based on nonlinear implicit equations, using numerical methods is usually essential, which requires relatively high computational cost and solid background knowledge [45]. There have been many software packages, such as Simulink [46], Pysyst [47], etc., to solve this problem. Although these programs provide user-friendly interfaces, component-based operating processes, and fancy post-process, they either neglect the reverse-biased effect or cannot treat detailed shading patterns as stated above [40,48]. Most importantly, their computational efficiency is relatively low and simulation settings may be very tedious in treating large systems [19]. Thus, they are not the general means of modeling large PV systems under PSC. Recently, data-driven methods are also utilized in simulating PV systems under PSC; typical examples include artificial neural networks (ANN), support vector machine (SVM), and Gaussian process regression (GPR) [49,50]. In theory, these methods can provide results very quickly with sufficient training. However, due to the complexities of the PSC, such methods only work well in some coarse analyses. Another inherent disadvantage is the non-interpretability of these methods, indicating that they cannot conduct in-depth analysis and guide further optimization. So far, ECM with proper numerical methods should be the only choice to characterize the electrical performance of PV under the complex real-world PSC. However, a high-efficiency and strong-robustness algorithm to solve this problem is still lacking.

1.2.3. Research gaps

Based on the literature review, the current modeling methods, as well as their applicability, advantages, and disadvantages, are summarized in Table 1. As indicated, a holistic, in-depth understanding of the PV system under PSC requires a full consideration of reverse-biased behaviors, the varieties of PV technologies, the diversities of system topologies, and the diversity of shading patterns. Importantly, these aspects should be incorporated into a computational-efficient architecture. However, to the best of our knowledge, there is no existing research that can fulfill these requirements simultaneously. A complete solution to this problem is still in high demand in both academia and industry.

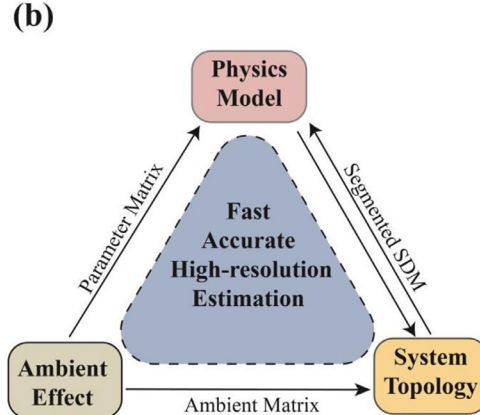
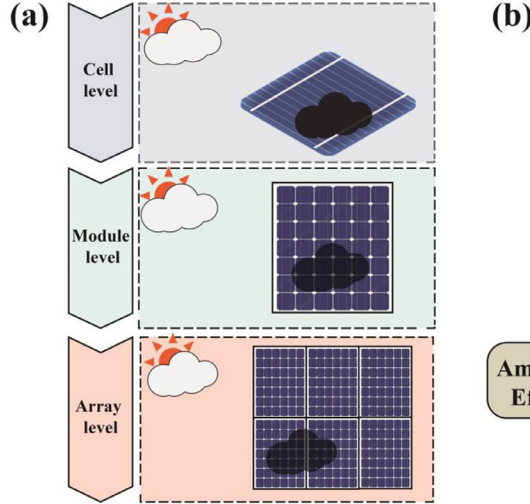
1.3. Novelties and contribution

Herein, an innovative model working inside a bottom-up architecture is presented to provide a generalized solution to this problem. This is achieved by the following novelties. Firstly, a novel segmented SDM (SSDM) with the ability to simulate both forward and reverse biased behaviors of a solar cell is presented. Secondly, SSDM is stacked via an efficient architecture to form the physics models of module and array, in which the system complexities and shading pattern diversities are fully considered. Lastly, multiple measures to enhance the simulation efficiency and facilitate coding are proposed at different scales. The effectiveness of the proposed method is validated via experimental data and mature software package thoroughly at different scales. The exclusive advantages of the proposed method are demonstrated via well-designed case studies. This method allows for the simulation of electrical behaviors of the PV system in the complex real world, which can facilitate the R&D of high-efficiency and long-lifespan PV systems.

Table 1

Summary of the methods in modeling PV performance under PSC.

Method	Applicability	Advantages	Disadvantages	Ref.
Traditional ECM-based	• Module • Array	• Simplicity	• Reverse-biased behaviors are neglected • Low accuracy • Low resolution in arrays	[15–19]
Bishop-based	• Cell • Module • Array	• Reverse-biased behaviors are considered • Capable of hot spot analysis	• Most focus on the cell-level • High computational cost • Some studies neglect the topology complexities	[21–24]
Component-based	• Module • Array	• User-friendly interface • Straightforward modeling workflow • Fancy post-processing	• Reverse-biased behaviors are neglected • Low resolution in arrays • License cost	[39,40]
AI-based	• Cell • Module • Array	• Simplicity • Low computational cost • Background knowledge is not essential	• Non-interpretability • The availability of training data • Low accuracy • Low resolution in arrays	[42,43]

**Fig. 1.** The roadmap of the methodology. (a) bottom-up architecture. (b) modeling techniques at each level.

1.4. Article structure

This paper is organized into five sections. A mathematical expression of the proposed method, as well as the numerical treatment, are developed in [Section 2](#). The validation settings and results of the proposed approach are detailed in [Section 3](#). Two case studies are conducted and analyzed in [Section 4](#) to furtherly demonstrate the advantage of the method. The key conclusions and outlooks are presented in [Section 5](#).

2. Methodology

From the scale of the photovoltaic system, it can be divided into cell-level, module-level, and array-level. Each scale has its complexity and is interconnected closely with other levels. Following a bottom-up architecture ([Fig. 1\(a\)](#)), the mentioned challenges and complexities in the previous section are addressed step by step in the proposed method. To achieve this, as is shown in [Fig. 1\(b\)](#), multiple improvements in both modeling and numerical treatment are proposed at each scale to finally achieve high simulation efficiency and flexibility without losing accuracy. The followings are the details of the methodology as well as the numerical treatment at each scale.

2.1. Cell modeling

Since the solar cell is the basic unit of power generation in a PV system, accurate determination of its electrical behaviors is the building bricks for further modeling.

2.1.1. Physics model

As is shown in [Fig. 2\(a\)](#), depending on the current flow through the cell, an operating solar cell can either be forward biased or reverse biased. Usually, when a PV module is under PSC, the shaded cells can be reverse biased since the generated current is lower than that of the unshaded cells. By solving the ECM ([Fig. 2\(b\)](#)), the I-V characteristic can be obtained ([Fig. 2\(c\)](#)). Notably, the product of the I and V refers to the power output of the solar cell. For forward biased mode, it always has a positive power output since its I-V curve is in the 1st quadrant. Conversely, the reverse biased mode has a negative output because its I-V curve is in the 2nd quadrant [29]. The followings are the details of the ECM.

The SDM model has been widely used in simulating the behavior of the forward-biased cell [45,51]. As is shown in the blue box of [Fig. 2\(b\)](#), it consists of a current source, a diode, a parallel resistance, and a series resistance. Using Kirchhoff's law, the output current of the cell I^c can be calculated using Eq. (1):

$$I^c = I_{ph}^c - I_d^c - I_p^c = I_{ph}^c - I_o^c \left[\exp \left(\frac{V^c + I^c R_s^c}{V_t^c} \right) - 1 \right] - \frac{V^c + I^c R_s^c}{R_p^c} \quad (1)$$

where the superscript c denotes the cell, I_{ph}^c is the photocurrent generated by the incident solar radiation in one solar cell, I_d^c is the current flowing through the diode, I_p^c is the current flowing through the parallel resistance, I_0^c is the reverse saturation current, V^c is the output voltage of the cell, $V_t^c = \gamma k_B T_c / q$ is the thermal voltage of the diode, γ is the ideality factor of the diode, k_B is the Boltzmann constant (1.3806503×10^{23} J/K), T_c is the temperature of solar cell calculated in the thermal model,

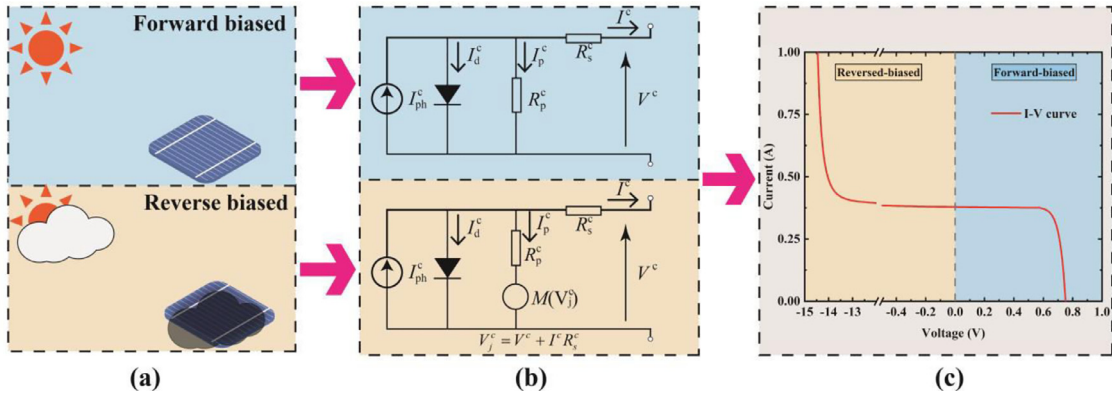


Fig. 2. The modeling at the cell level. (a) operating conditions. (b) segmented SDM. (c) electrical characteristics.

q is the electron charge ($1.60217646 \times 10^{-19}$ C), R_s^c and R_p^c are the series resistance and parallel resistance, respectively.

Despite its high accuracy and computational efficiency, traditional SDM cannot model the behaviors of the reverse biased cell. To address this issue, some scholars developed an enhanced SDM (ESDM) in which a voltage-controlled current source is added to SDM, representing the negative diode breakdown operation [25,26]. The circuit diagram is shown in the yellow box of Fig. 2(b); using Kirchhoff's law, the output current I can be calculated using Eq. (2):

$$I^c = I_{ph}^c - I_o^c \left[\exp \left(\frac{V^c + I^c R_s^c}{V_t^c} \right) - 1 \right] - \frac{V^c + I^c R_s^c}{R_p^c} \left[1 + a \left(1 - \frac{V^c + I^c R_s^c}{V_{br}} \right)^{-m} \right] \quad (2)$$

where a is the fraction of current involved in avalanche breakdown, V_{br} is the junction breakdown voltage, m is the avalanche breakdown exponent.

Theoretically, ESDM is a complete method for simulating the behaviors of solar cells. However, the high computational cost limits its applicability in simulating large PV systems. This is because the introduced term in ESDM significantly increases the transcendental and implicit features of SDM. Herein, considering that the traditional SDM already has outstanding performance in the forward-biased region, a segmented SDM combining the traditional SDM and the ESDM is proposed to achieve a balance between accuracy and efficiency. As illustrated in Fig. 2(c), using this method, the I-V characteristics of the solar cell can be obtained in sections. The formula is shown in Eq. (3) and the optimal numerical treatment is presented in the following sections.

$$I^c = \begin{cases} I_{ph}^c - I_o^c \left[\exp \left(\frac{V^c + I^c R_s^c}{V_t^c} \right) - 1 \right] - \frac{V^c + I^c R_s^c}{R_p^c} i f I^c \leq I_{sc}^c \\ I_{ph}^c - I_o^c \left[\exp \left(\frac{V^c + I^c R_s^c}{V_t^c} \right) - 1 \right] - \frac{V^c + I^c R_s^c}{R_p^c} \left[1 + a \left(1 - \frac{V^c + I^c R_s^c}{V_{br}} \right)^{-m} \right] i f I^c > I_{sc}^c \end{cases} \quad (3)$$

where I_{sc}^c is the short circuit of the solar cell.

2.1.2. Parameters extraction

To complete the cell model, the unknown parameters in Eq. (3), i.e., I_{ph}^c , I_o^c , V_t^c , R_s^c , R_p^c , a , V_{br} , and m , should be determined. For parameters related to the avalanche effect (a , V_{br} , and m), previous studies [26,27,29] have evidenced that using constant value is accurate enough. The other five parameters can be extracted from standard testing conditions (STC) data via analytical methods, numerical iteration, or meta-heuristic algorithms [52]. In this paper, an extraction method published in our previous studies is used [45]. If the datasheet values of the solar cell are not available, the STC parameters of the module can be extracted firstly via the same method, and then using the following equations to

obtain the STC parameter of the cell:

$$\begin{cases} I_{ph,stc}^c = I_{ph,stc}^m / N_p \\ I_{o,stc}^c = I_{o,stc}^m / N_p \\ V_{t,stc}^c = V_{t,stc}^m / N_S \\ R_{s,stc}^c = R_{s,stc}^m N_p / N_s \\ R_{p,stc}^c = R_{p,stc}^m N_p / N_s \end{cases} \quad (4)$$

where $I_{ph,stc}^m$, $I_{o,stc}^m$, $V_{t,stc}^m$, $R_{s,stc}^m$, and $R_{p,stc}^m$ are the five parameters of the module, N_p and N_s are the number of cells connected in parallel and series in a module, respectively.

2.1.3. Ambient effect

When the PV operates under general conditions (GC), the parameters will be different from the values under STC. Taking the STC parameter as a reference, the parameters under GC can be obtained by considering the dependence on the cell temperature and solar irradiance [45]:

$$\begin{cases} I_{ph}^c = \left(I_{ph,stc}^c + K_i \Delta T \right) \frac{G^c}{G_{stc}} \\ I_o^c = \frac{I_{o,stc}^c + K_v \Delta T}{\exp \left[\left(V_{oc,stc}^c + K_v \Delta T \right) / V_{t,stc}^c \right] - 1} \\ V_t^c = V_{t,stc}^c \frac{T^c}{T_{stc}} \\ R_s^c = R_{s,stc}^c \\ R_p^c = R_{p,stc}^c \frac{G^c}{G_{stc}} \end{cases} \quad (5)$$

where the subscript stc represents the STC, K_i is the short-circuit current temperature coefficient, $\Delta T = T^c - T_{stc}$ is the temperature difference between the GC and STC, G^c is the irradiance on the solar cell, I_{sc}^c is the short-circuit current of the cell, V_{oc}^c is the open-circuit voltage, K_v denotes open-circuit voltage temperature coefficient.

Notably, when the cell is shaded, the G^c is different from the irradiance on the cell. To quantify this effect, the shading factor ω is defined in Eq. (6), which means the ratio between the G^c and the irradiance on the cell.

$$\omega = \frac{G^c}{G} \quad (6)$$

Since these parameters are highly dependent on the temperature, it is important to include an effective temperature model. In this research, the nominal operating cell temperature (NOCT) model is adopted, which is considered one of the most efficient temperature models [40]. The model is expressed by Eq. (7):

$$T^c = T_a + (T_{NOCT} - T_{a,NOCT}) \cdot \frac{G^c}{G_{NOCT}} \quad (7)$$

where T_a is the ambient temperature, T_{NOCT} is the NOCT temperature, which is a module parameter, $T_{a,NOCT}$ and G_{NOCT} refer to the NOCT condition (20°C and 800 W/m^2).

2.1.4. Numerical treatment

The developed physics model for the cell is a segmented equation with transcendental and implicit features, thus using a numerical method is essential. Although previous studies have evidenced the effectiveness of the Newton-Raphson method (NRM) in solving such a problem, the convergence speed of NRM is highly associated with the initial value [19]. Considering the features of Eq. (3), a segmented NRM is proposed in this study. Importantly, different from the customary to set zero as the initial value in many previous studies [45,53]. The ambient-dependent initial values in each region (forward or reverse) are used, which aims to achieve high computational stability and efficiency. The followings are the detailed steps of the numerical treatment, and a step-by-step coding instruction with flowchart illustration is presented in [Algorithm 1](#) and [Fig. S1 in Supplementary file](#).

- (1) Transforming Eq. (3) into a function $f(V^c)$, the problem becomes solving the equation $f(V^c) = 0$:

$$f(V^c) = \begin{cases} I_{ph}^c - I_o^c \left[\exp\left(\frac{V^c + I^c R_s^c}{V_t^c}\right) - 1 \right] - \frac{V^c + I^c R_s^c}{R_p^c} - I^c i f I^c \leq I_{sc}^c \\ I_{ph}^c - I_o^c \left[\exp\left(\frac{V^c + I^c R_s^c}{V_t^c}\right) - 1 \right] - \frac{V^c + I^c R_s^c}{R_p^c} \left[1 + a \left(1 - \frac{V^c + I^c R_s^c}{V_{br}} \right)^{-m} \right] \\ \quad - I^c i f I^c > I_{sc}^c \end{cases} \quad (8)$$

- (2) Calculating the derivative of $f(V^c)$:

$$f'(V^c) = \begin{cases} -\frac{I_o^c}{V_t^c} \exp\left(\frac{V^c + I^c R_s^c}{V_t^c}\right) - \frac{1}{R_p^c} i f I^c \leq I_{sc}^c \\ -\frac{I_o^c}{V_t^c} \exp\left(\frac{V^c + I^c R_s^c}{V_t^c}\right) - \frac{1}{R_p^c} \left[1 + a \left(1 - \frac{V^c + I^c R_s^c}{V_{br}} \right)^{-m} \right] - \\ \frac{ma}{V_{br}} \left(\frac{V^c + I^c R_s^c}{V_t^c} \right) \left(1 - \frac{V^c + I^c R_s^c}{V_{br}} \right)^{-m-1} i f I^c > I_{sc}^c \end{cases} \quad (9)$$

- (3) Selecting the current point at a regular interval in $[0, I_{sc}^c]$ and computing the corresponding voltage value via NRM with selected initial values V_0^c :

$$V_{i+1}^c = \begin{cases} V_i^c - \frac{f(V_i^c)}{f'(V_i^c)} \text{ with } V_0^c = V_{oc}^c \text{ if } I^c > I_{sc}^c \\ V_i^c - \frac{f(V_i^c)}{f'(V_i^c)} \text{ with } V_0^c = V_{br}^c \text{ if } I^c \leq I_{sc}^c \end{cases} \quad (10)$$

where the subscript i is the i^{th} iteration step in the NRM, V_0^c is the initial value of the iteration. The iteration will continue several times until the tolerance is met. The I-V curve of the solar cell under certain operating conditions can thus be determined. Moreover, by computing the product of current and voltage, the P-V curve can be obtained easily and MPP can be found subsequently via the ‘max’ function in programming languages.

2.2. Module modeling

PV module is the assembly of solar cells to achieve the desired voltage and current. Each module consists of several PV cell strings (CS) and each string is a collection of several cells in series. Normally a BPD is connected in parallel to the CS to alleviate the power mismatch and the hot spot effect [26,29].

2.2.1. Physics model

[Fig. 3](#) is an example to show the modeling method for the PV module under PSC. As is shown in [Fig. 3\(a, b\)](#), the non-uniform irradiance on the module leads to a different irradiance distribution in the CSs. CS 1 contains several shaded cells while the cells in CS 2 and CS 3 receive uniform irradiance. As a result, the I-V curve shows a staircase due to the activation of the BPD of CS 1 ([Fig. 3\(c\)](#)).

To model the electrical behaviors of the PV module, the electrical behaviors of the CS should be determined first. Depending on the state

of the BPD, there are two cases. For the non-shaded strings, every cell generates the same current and there is no reverse biased cell. As a result, the BPD in parallel is not activated and the voltage of the CS is just the sum of the cells. On the other hand, in the CS under PSC, the cells with lower irradiance can be reverse biased if the module current is larger than their short-circuit currents, generating the negative voltage and sinking the power from the other cells. In this case, if the voltage drop is not significant, i.e., the BPD is still non-activated, the voltage of the string is still the sum of the cells. However, when the voltage drops down to a threshold V^{BPD} (typically -0.7 V for silicon BPD), the BPD activates and the corresponding CS is protected. Then the voltage of the string is equal to the threshold value. The above working principles can be expressed using the following equation:

$$V_i^{cs} = \begin{cases} V^{BPD} \text{ if } V_i^{cs} \leq V^{BPD} \\ \sum_{j=1}^n V_j^c \text{ else} \end{cases} \quad (11)$$

where the superscript cs denotes the CS, V_i^{cs} is the voltage of the i^{th} CS, V^{BPD} is the threshold voltage of the BPD, V_j^c is the voltage of the j^{th} cell in the string, it can be obtained using the cell model method in the previous section, n is the number of cells in the CS.

After obtaining the voltage of each CS, the module voltage can be calculated using Eq. (12):

$$V^m = \sum_{i=1}^k V_i^{cs} \quad (12)$$

where the superscript m denotes the module, k is the number of CSs in the module.

2.2.2. Ambient matrix

As indicated above, the module’s electrical characteristic is determined by both the CS and the BPD. To facilitate the consideration of the ambient effect on each solar cell, an efficient way to organize the ambient parameter should be proposed. Herein, the ambient matrix considering the effects of shadow and temperature is proposed. The cells in the module are numbered and their corresponding shading information and temperature are organized as a shading matrix Ω^M and T^M , respectively. The expression of the two matrixes is detailed in [Appendix A.1](#).

2.2.3. Parameter matrix

The non-uniform ambient effect causes an inhomogeneous distribution of the cell’s parameters. Thus, the parameters of each cell are calculated using Eq. (5) with the corresponding parameter from the constructed Ω^M and T^M . Then, they are also organized in matrix form to facilitate the solution process. The expression of these matrixes is detailed in [Appendix A.2](#).

2.2.4. Numerical treatment

After constructing the physics model, parameter matrix, and ambient matrix, the electrical characteristics of the PV module can be accurately estimated. In short, the numerical treatment of this step is to obtain the I-V characteristic of each cell and then obtain the CS characteristics following the principle in the physics model. To present its detailed steps and the logical structure, a step-by-step coding instruction with flow chart illustration is given in [Algorithm 2](#) and [Fig. S2 in the Supplementary file](#).

2.3. Array modeling

In engineering practice, modules are usually electrically interconnected to form an array to obtain the desired voltage and current. In this regard, the means of interconnection plays a significant role in optimizing the power output of a large system, especially when PSC occurs. The series-parallel (SP) array topology with central inverters is the most popular choice in a large PV system for its simplicity in installation and low

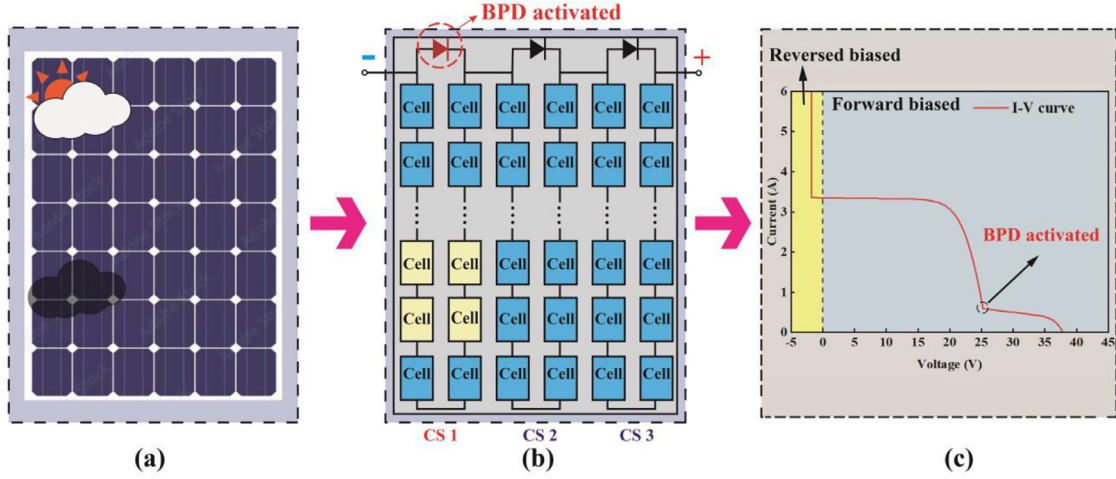


Fig. 3. The modeling method at the module level. (a) operating condition. (b) irradiance distribution. (c) electrical characteristics.

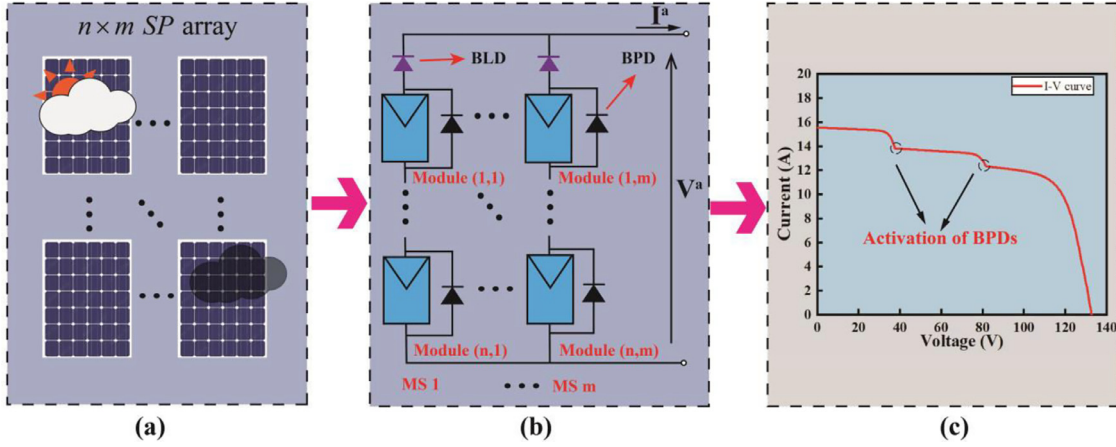


Fig. 4. The modeling method at the array level. (a) scheme of the operating condition. (b) array topology. (c) example of electrical characteristics.

initial cost [41]. In addition, SP topology includes all important features of a large array, such as the serial-parallel connection, BPD connected with the module, and blocking diode (BLD). Considering its dominance and representativeness in the market, it is used in this section to demonstrate the working principles of the array-level model. Notably, the same principles can be generalized to other topologies as well.

2.3.1. Physics model

Fig. 4(a) shows the scheme of an $n \times m$ SP array operating under PSC and the detailed electrical topology is shown in Fig. 4(b), in which there are m module strings (MS) connected in parallel and each MS has n PV modules connected in series. Moreover, BPD is connected in parallel with each module to mitigate the PSC adverse effect. There is a BLD connected in series at the end of each MS to prevent the current from flowing backward. As is shown in Fig. 4(c), the two measures can ensure the array have an I-V characteristic in the first quadrant, i.e., the array always serves as a power generator. Like the module cases, the I-V characteristics also show the features of the staircase due to the implementation of the BPD. The followings are the details of the physics model of the SP array.

In each MS, the current of each module is the same due to the serial connection and the voltage follows the relationship expressed by Eq. (13):

$$V_j^{ms} = \sum_{i=1}^n V_{i,j}^m + V^{BLD} \quad (13)$$

where the superscript ms denotes the MS, V_j^{ms} is the voltage of the j^{th} module string, $V_{i,j}^m$ is the voltage of the i^{th} module in the j^{th} module string, which can be calculated using Eqs. (11) and (12), V^{BLD} is the voltage drop in the BLD (about -0.7 V).

Because the array consists of several MSs connected in parallel, its voltage V^a and current I^a follow the followings relationship:

$$V^a = V_j^a \quad (14)$$

$$I^a = \sum_{j=1}^n I_j^{ms} \quad (15)$$

where the superscript a denotes the array, V^a and I^a are the voltage and the current of the array, respectively. I_j^{ms} is the current in the j^{th} module string.

Eqs. (13)–(15) form the physics model of an SP array. The I-V characteristics can be estimated by applying the model based on the calculation results from the developed cell and module models. The application details are detailed in the following subsections.

2.3.2. Generalized ambient matrix

As indicated above, the electrical characteristics of a PV array are determined by each module as well as the states of BPDs and BLDs. Since the solar cell is the basic unit for simulation and there are a large number of solar cells in the array, an efficient way to organize the ambient information should be proposed. Herein, the ambient matrix proposed at the module level is generalized to an array in which the modules in

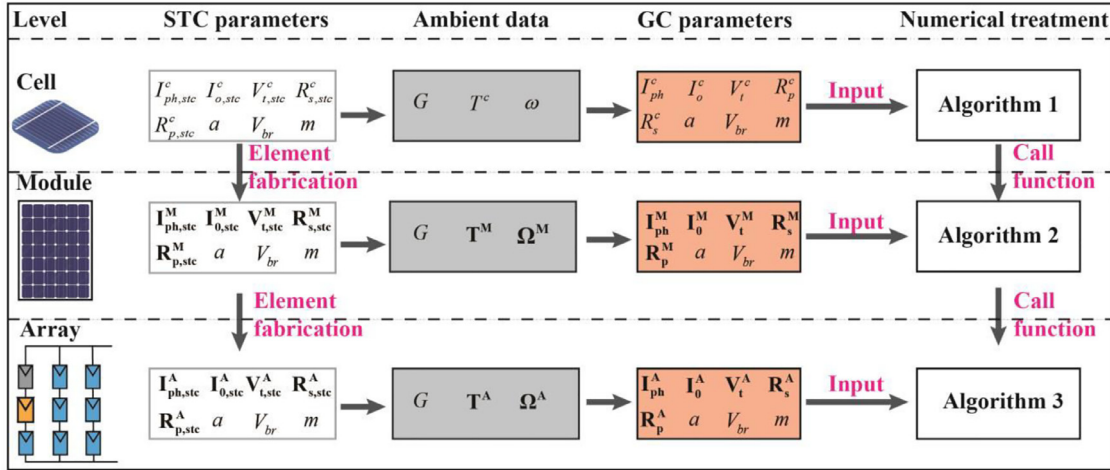


Fig. 5. The cell-module-array interdependence and simulation workflow.

the array are numbered and their shading information and temperature are contained in two generalized matrices: Ω^A and T^A . This treatment provides an efficient way to organize and store the ambient parameter mathematically. Moreover, it can be handily achieved by some data structures in programming languages, such as the cell or structure in MATLAB and structure in JAVA language. The expression and detailed description of the two generalized matrixes are detailed in Appendix B.1.

2.3.3. Generalized parameter matrix

Similarly, it is natural to organize the cell's parameter following the form of the generalized ambient matrix. This can be achieved by generalizing the proposed parameter matrix in Section 2.2.3. The mathematical expression and detailed description of the two generalized matrixes are detailed in Appendix B.2.

2.3.4. Numerical treatment

After constructing the physics model, generalized ambient matrices, and parameter matrices, the electrical characteristics of the array can be accurately estimated. The idea is in general very similar to that in the module treatment: solving the physics model of each cell in the array and then following the calculation principle presented in the physics models of module and array progressively. To present its detailed steps and the logical structure, a step-by-step coding instruction with flowchart illustration is given in Algorithm 3 in the Supplementary file.

2.4. Workflow and interdependence

The general simulation workflow and interdependence of the complete method are summarized in this subsection. As is shown in Fig. 5, this workflow follows the same sequence. The STC parameters are determined firstly via parameter extraction. Then, the STC parameters are transformed into the GC parameter with the ambient data. Finally, the GC parameters are loaded into the numerical treatment to obtain the solution.

Since the low-level system can be regarded as a subsystem of the high-level one, there are cell-module and cell-module-array interdependence in both model parameter preparation and model solution. Taking Algorithm 2 as an example, the STC matrix can be created via the fabrication of the STC parameters, which have been defined in Algorithm 1. After obtaining the GC matrix at given ambient conditions, the I-V characteristic is calculated cell by cell by calling Algorithm 1 in a loop. Similar dependence also exists in array-level modeling, which has been detailed in Algorithm 3.

Table 2

Main computational environment for simulation.

Configurations	Parameter
CPU	Intel(R) Xeon(R) 5218 CPU @ 2.30GHz
RAM	128 GB
SSD	2 TB
Operating system	Windows 10

3. Validation

To systematically validate the effectiveness of the proposed method, a rigorous, progressive validation process is designed and conducted. Fig. 6 shows the roadmap of the validation process. Firstly, at the cell level, the proposed method is validated against the measurement data of the solar cells with mainstream PV technologies to test its accuracy, efficiency, and applicability. Moreover, the proposed method is validated against the measurement data of a commercial PV module in eight different shading scenarios. Lastly, the capability of the proposed method to simulate the PV array is tested and compared with the Simulink. All simulation is programmed in MATLAB R2021b and the main computational environment is presented in Table 2. The absolute error ϵ at MPP is used to quantify the accuracy of the method. The expression is shown in Eq.(16). The elapsed time t determined by the 'tic toc' function in MATLAB is used to quantify the performance of the proposed method. All simulation results against the measurement data can be found in the Excell sheet in Appendix C.

$$\epsilon = |P_{sim} - P_{mea}| \quad (16)$$

where ϵ is the absolute error, P_{sim} is the simulated power at MPP, P_{mea} is the measured power at the MPP.

3.1. Cell level

3.1.1. Validation settings

To make sure the cell model can be applied to wide technologies in the PV industry, three mainstream technologies in the market are selected, including (1) monocrystalline silicon, (2) polycrystalline silicon, and (3) thin-film technology based on CuInS₂. Both forward and reverse biased regions were measured under well-controlled environments as suggested by Restrepo-Cuestas et al. [54]. The parameters, as well as the operating condition used in the cell model, are listed in Table S1.

3.1.2. Validation results

Fig. 7 shows the validation results at the cell level. As indicated, regardless of the cell technologies, good agreement is obtained be-

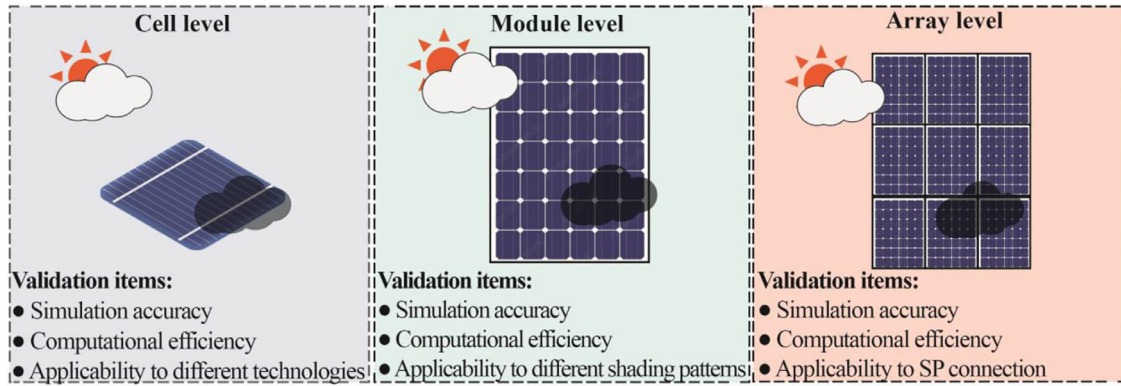


Fig. 6. Roadmap of the validation process.

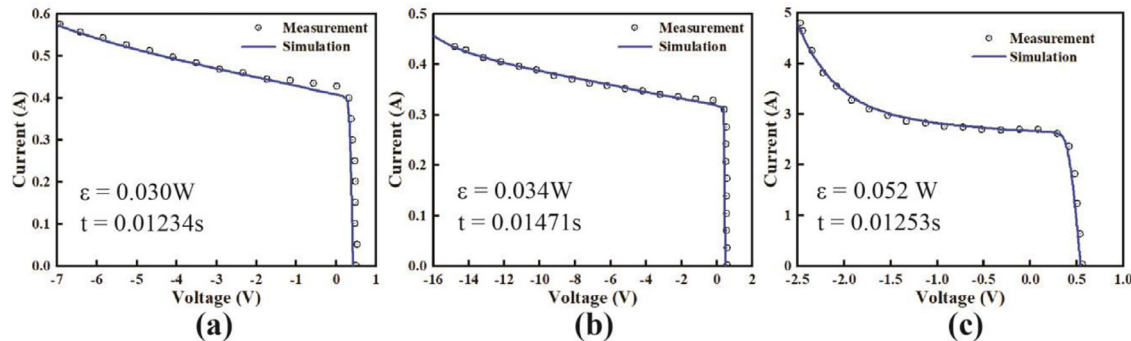


Fig. 7. Validation results at the cell level. (a) monocrystalline silicon cell. (b) polycrystalline silicon cell. (c) thin-film cell.

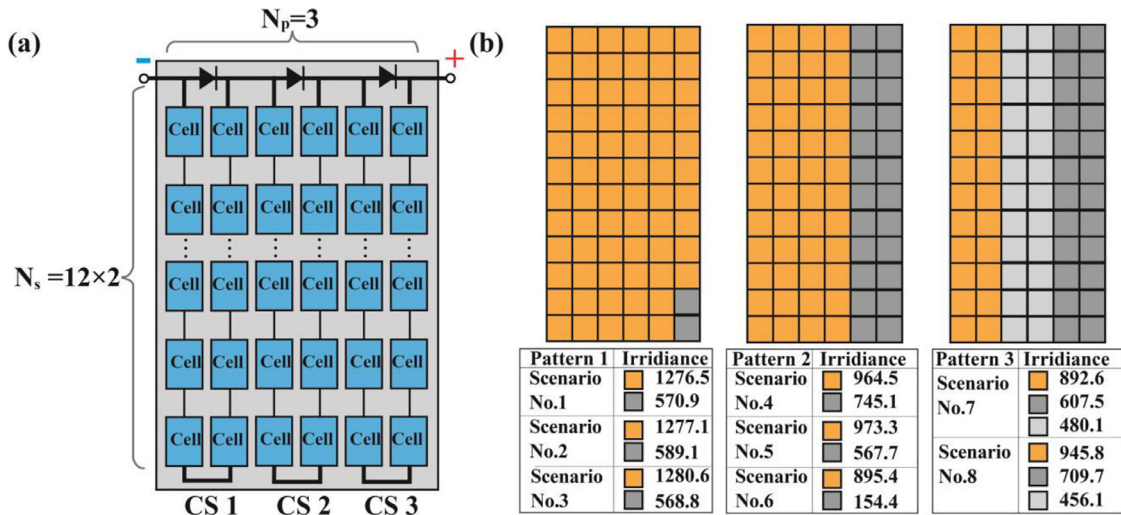


Fig. 8. Validation settings at the module level. (a) scheme of the PV module. (b) shading scenario settings.

tween the simulation and measurement with an absolute error within 0.052 W at MPPs. Importantly, all the I-V curves show uprising trends in the reversed biased region, but the trend of the thin-film cell (Fig. 7(c)) is much sharper due to the relatively small breakdown voltage. On top of the high accuracy, the elapsed time of all validation is within 0.01471s. Generally, these good results demonstrate the accuracy and efficiency of the SSDM and segmented NRM. It can be concluded that the proposed method is valid at the cell level, which can be a basic component for further module- and array-level simulation.

3.2. Module level

3.2.1. Validation settings

Besides the accuracy and efficiency, the capability to treat different shading patterns needs fully testing at the module-level validation. To this, measurement data of a commercial monocrystalline silicon module are used [27]. As is shown in Fig. 8(a), this module contains three CSs with a BPD connected in parallel to each. There are 24 solar cells connected in series in each string. The extracted parameters of the cell are shown in Table S2. As is shown in Fig. 8(b), there are three shading

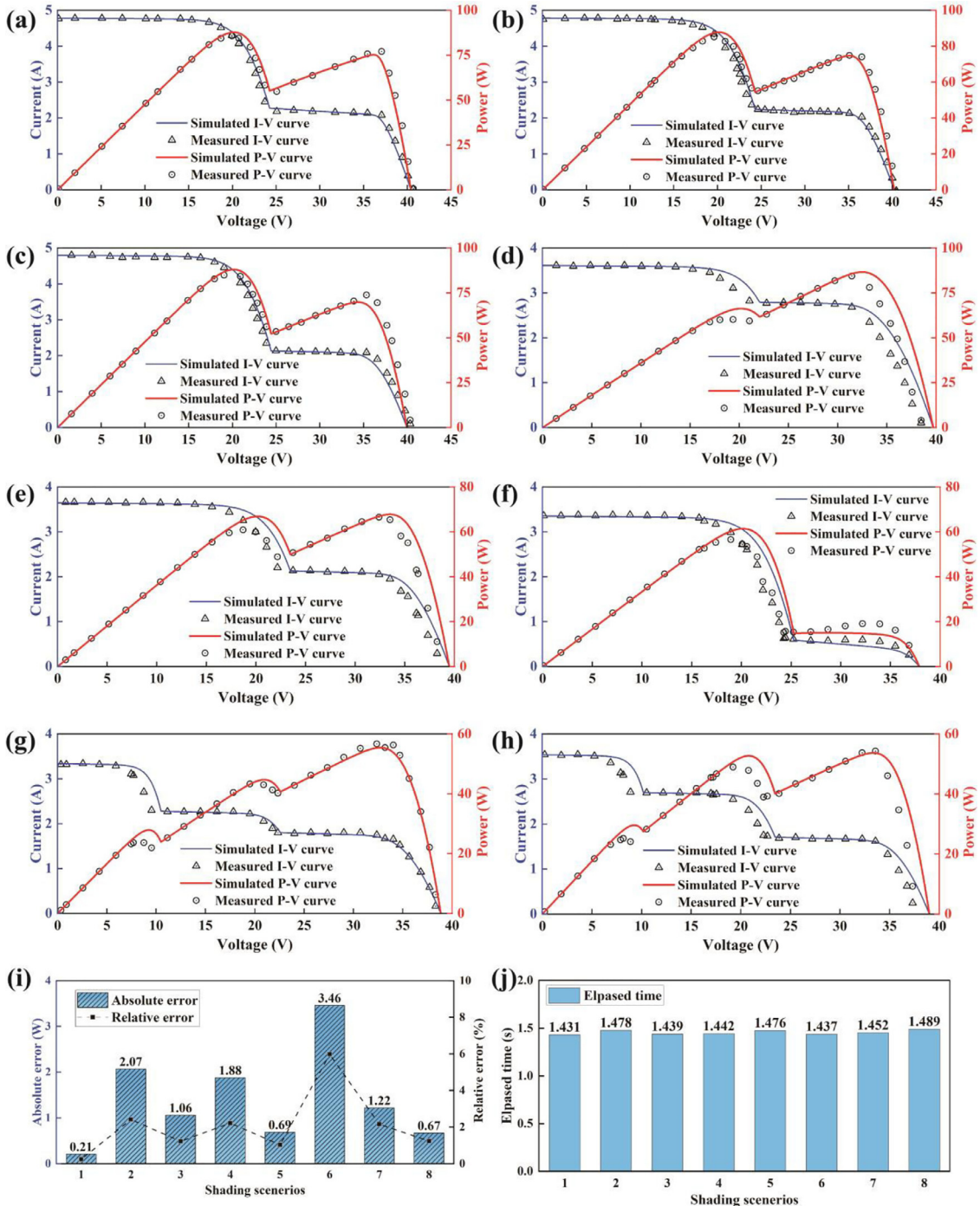


Fig. 9. Validation results at the module level. (a) scenario 1. (b) scenario 2. (c) scenario 3. (d) scenario 4. (e) scenario 5. (f) scenario 6. (g) scenario 7. (h) scenario 8. (i) error analysis results at MPP. (j) elapsed time.

patterns used for validation. Furthermore, the three can be classified into 8 shading scenarios: (1) scenarios No.1–3, 2 cells in string 3 are shaded; (2) scenarios No.4–6, string 3 is fully shaded; (3) scenarios No.7–8, both string 2 and 3 are fully shaded.

3.2.2. Validation results

Fig. 9(a–c) shows the results of scenarios 1–3 in which two cells in the 3rd string are shaded. As indicated, the simulated I-V curves and P-V curves are highly consistent with the measurement data. When the module current is higher than the short-circuit current of the shaded cell (about 2 A), the shaded cells in the 3rd CS are reverse biased. The gen-

erated negative voltage begins to drop down the voltage of the whole string and the connected BPD will activate when the string voltage reaches the threshold. As a result, there is a staircase in the I-V curves and the P-V curves show two MPPs correspondingly. Fig. 9(i) shows the absolute errors of the three scenarios at GMPP, which are 0.21 W, 2.07 W, and 1.06 W, respectively. The corresponding relative errors are all within 2.1%. In addition, the elapsed times for all simulations are within 1.478 s (Fig. 9(j)).

Fig. 9(d–f) shows the results of scenarios 4–6, in which the entire 3rd string is shaded with three different degrees. Similarly, the simulated I-V curves and P-V curves are highly consistent with the measure-

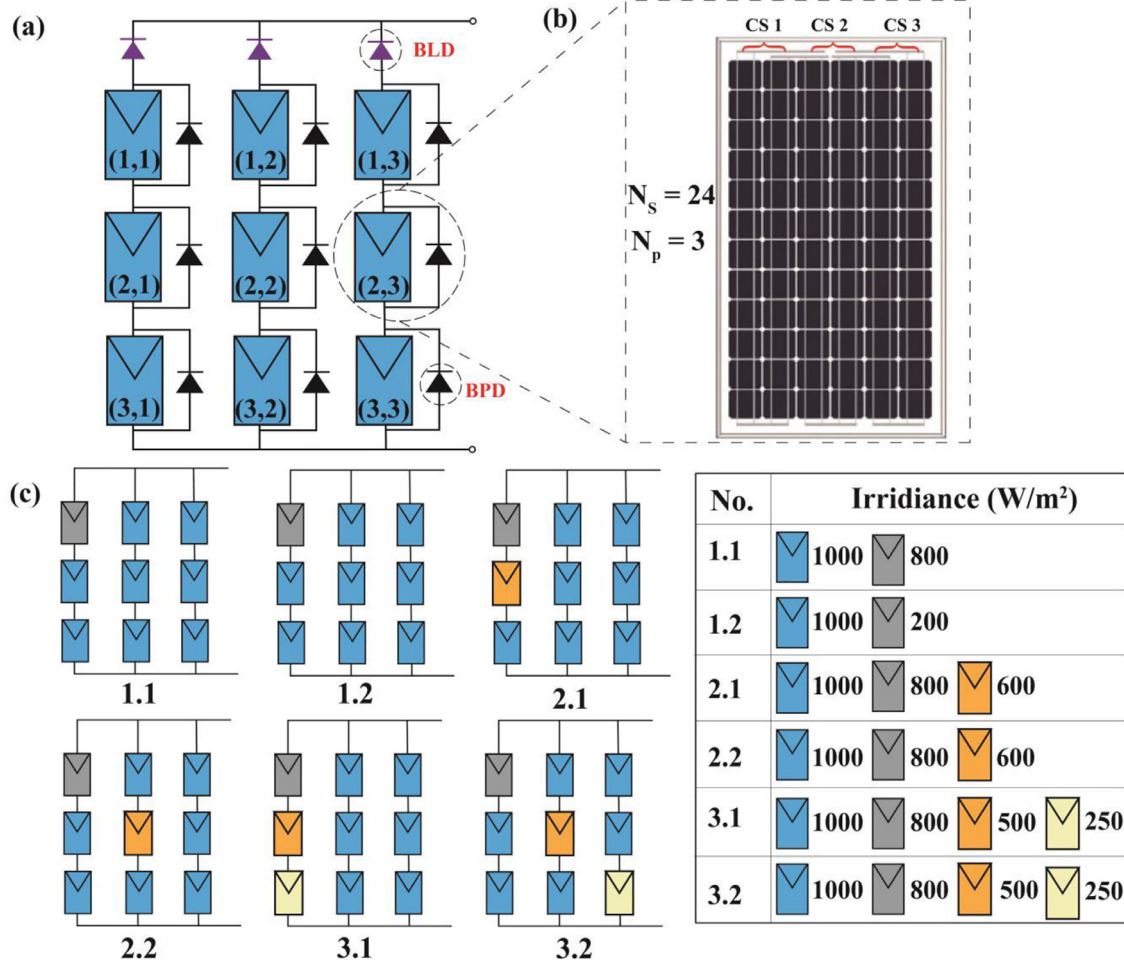


Fig. 10. Verification settings at the array level. (a) array topology. (b) LNPV-125*125-F/C module. (c) The setup of the PSC scenarios.

ment data. The similar two-staircase-shaped I-V curve and P-V curves with two MPPs are observed again. Due to the heavy shading, the short-circuit current and open-circuit voltage of the module are much lower than that of scenarios 1–3, thus leading to a significant drop at GMPP. Notably, as the shading factor decreases, the second staircase becomes lower. Fig. 9(i) shows the absolute errors of the three scenarios at GMPP, which are 1.88 W, 0.69 W, and 3.42 W, respectively. The corresponding relative errors are all within 6.07%. In addition, the elapsed times for all simulations are within 1.476 s (Fig. 9(j)).

Fig. 9(g–h) shows the results of scenarios 7–8, in which both 2nd and 3rd strings are shaded but with different degrees. The simulated curves agree well with the measurement values. Because there are three irradiance levels in the two scenarios, the BPDs of the 2nd and 3rd CS activate one by one as the module current increases. As a result, there are three staircases in the I-V curves, which is the most distinctive feature of the previous cases. Correspondingly, the P-V curves exhibit three MPPs increasing from the low voltage to high voltage. As presented in Fig. 9(i–j), the absolute error is within 1.22 W, the relative error is within 2.01%, and the elapsed time is within 1.489 s.

3.3. Array level

3.3.1. Validation settings

Based on the successful validation at cell and module levels, the proposed method to treat PV arrays needs testing. Since there is no available measurement data, a side-by-side comparison with experimentally validated software is a rational choice. Simulink has demonstrated high accuracy in simulating PV arrays with module-level PSC

in many studies. Thus, it was used as the benchmark in the validation. As is shown in Fig. 10(a), an SP array with 3×3 modules is used because it is a common topology in rooftop systems or community systems and it includes all important features (SP interconnection, BPD, BLD) of an array. Importantly, to make sure the verification is close to the real-world scenarios, a popular PV module named LNPV-125*125-F/C (Fig. 10(b)) is used in the array. The datasheet values and the extracted parameters are presented in Fig. S4 and Table S3. The setup of the SP array in Simulink is presented in Fig. S5. To fully test the performance of the proposed method, as is shown in Fig. 10(c), 6 PSC patterns following an order from simple to complicated are designed. Both Simulink and the proposed method are used to simulate these scenarios.

3.3.2. Validation results

Fig. 11(a1-a3) shows the verification results when the array is under PSC No. 1.1 and 1.2. As indicated in Fig. 11(a1-a2), the simulated curves agree well with the Simulink ones. The I-V curve shows a double staircase feature, but the second step of scenario 1.2 is much lower. Both P-V curves have two MPPs due to the activation of the BPD. Fig. 11(a3) shows the performance metrics of both scenarios. The GMPPs values of these two methods are very close within a maximum difference of 26 W, which verifies the accuracy of the proposed method. However, the elapsed time of the proposed method is nearly half of that of Simulink, indicating the high efficiency of the proposed method.

Fig. 11(b1-b3) shows the verification results when the array is under PSC No. 2.1 and 2.2. Good agreement is obtained again between the two methods. The I-V curve of scenario 2.1 shares the same feature as the

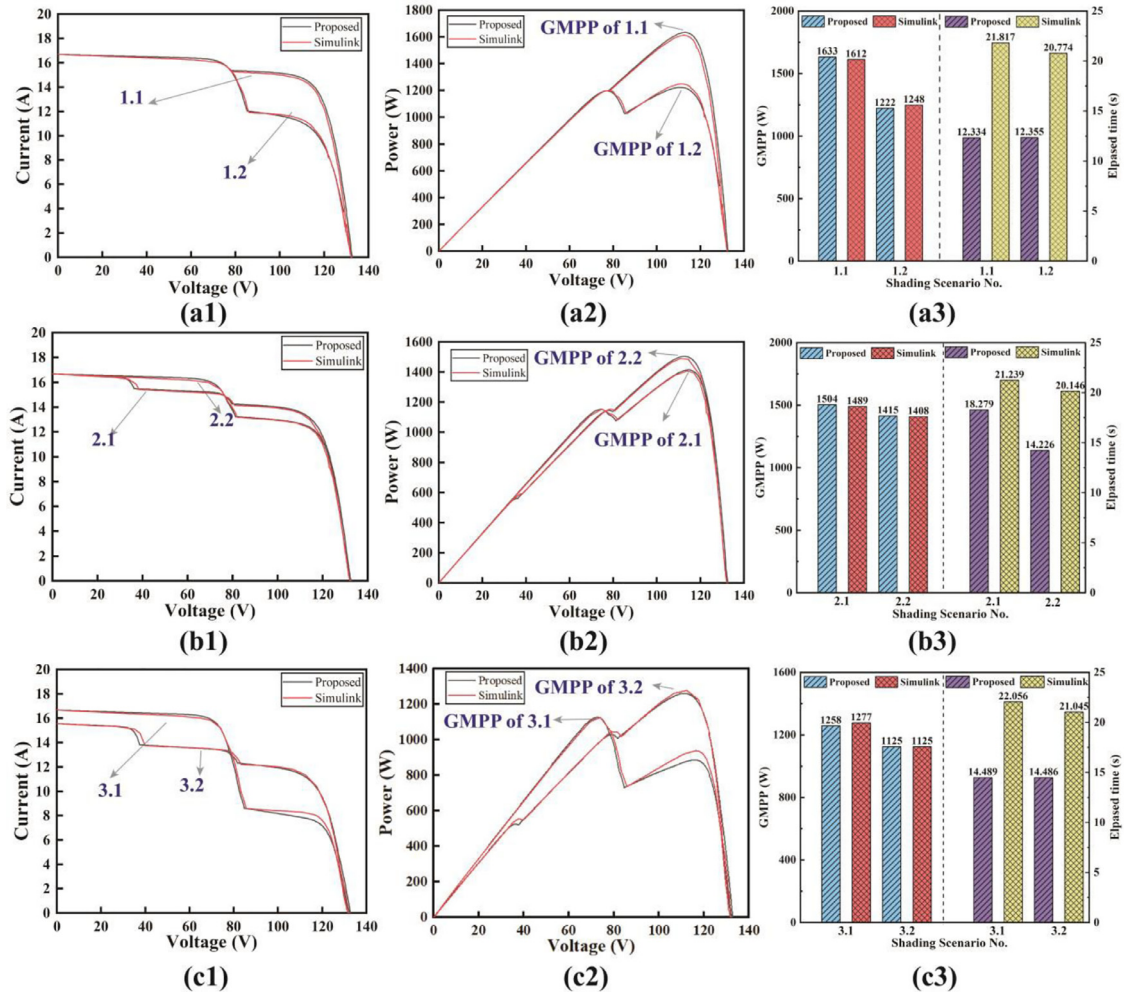


Fig. 11. Verification results at the array level. (a1-a3) scenario 1.1 and 1.2. (b1-b3) scenario 2.1 and 2.2. (c1-c3) scenario 3.1 and 3.2.

previous scenarios. But there is another staircase in the I-V curve of scenario 2.2 because the two shaded modules are not in the same MS. In Fig. 11(b2), there are three MPPs in the P-V curve of scenario 2.2 and the GMPP is slightly higher than that of scenario 2.1. As indicated in Fig. 11(b3), the GMPPs values of the two methods are very close within a maximum difference of 15 W and the elapsed time of the proposed method is 15–40% less than that of Simulink.

Fig. 11(c1-c3) shows the verification results when the array is under the shading patterns 3.1 and 3.2. Similarly, when the shaded modules are not in the same MS, there will be another staircase in the I-V curve and a peak in the P-V curve correspondingly (see Fig. 11(c1-c2)). Still, the maximum difference of calculated GMPPs is 19 W and the elapsed time of the proposed method is 40% less than that of Simulink.

3.4. Discussion of the validation results

As indicated, the proposed method achieves success in the above progressive, interdependent validation. At the cell level, the ability to simulate forward and reverse biased behaviors is justified in three solar cells with different technologies. Then, validation at the module level evidence that the proposed method can correctly simulate a commercial module with different shading patterns. Finally, a side-by-side comparison with Simulink is conducted at the array level. The proposed method can achieve Simulink's accuracy more efficiently. The high consistency also indicates that the behavior of each cell or module in the array and their electrical interconnection have been properly simulated.

Taking a comprehensive inspection of the entire validation, the proposed method considers the reverse biased effects, shading pattern nonuniformity, and PV topology diversity simultaneously at three levels. Because the validation nearly covers all important features in current PV practices, it could be concluded that the proposed method is an accurate and efficient tool to simulate the PV system in real-world scenarios.

4. Case studies

Besides the confirmed high accuracy, efficiency, and versatility, the proposed method has some exclusive abilities to model and analyze some complex scenarios. Herein, using the same module in Section 3.3, two case studies are designed to demonstrate this point.

4.1. Case 1: Hot spot risk assessment

The formation of the hot spot in the PV module is complex, which is not only determined by the PSC pattern but also by the module topology. Small-scale PSC, such as fallen leaves and bird droppings, is considered the major cause. For PV deployed in the urban context, shade from the surrounding buildings is another reason. Simultaneously, the severe heat island effect can aggravate hot spots posing underperformance and fire risks [55,56]. Assessment of the hot spot risk in advance is significant for finding mitigation solutions. Due to the neglect of reverse biased behaviors, it is challenging for existing methods to achieve this. Fortunately, the proposed method provides a complete solution to this problem. To

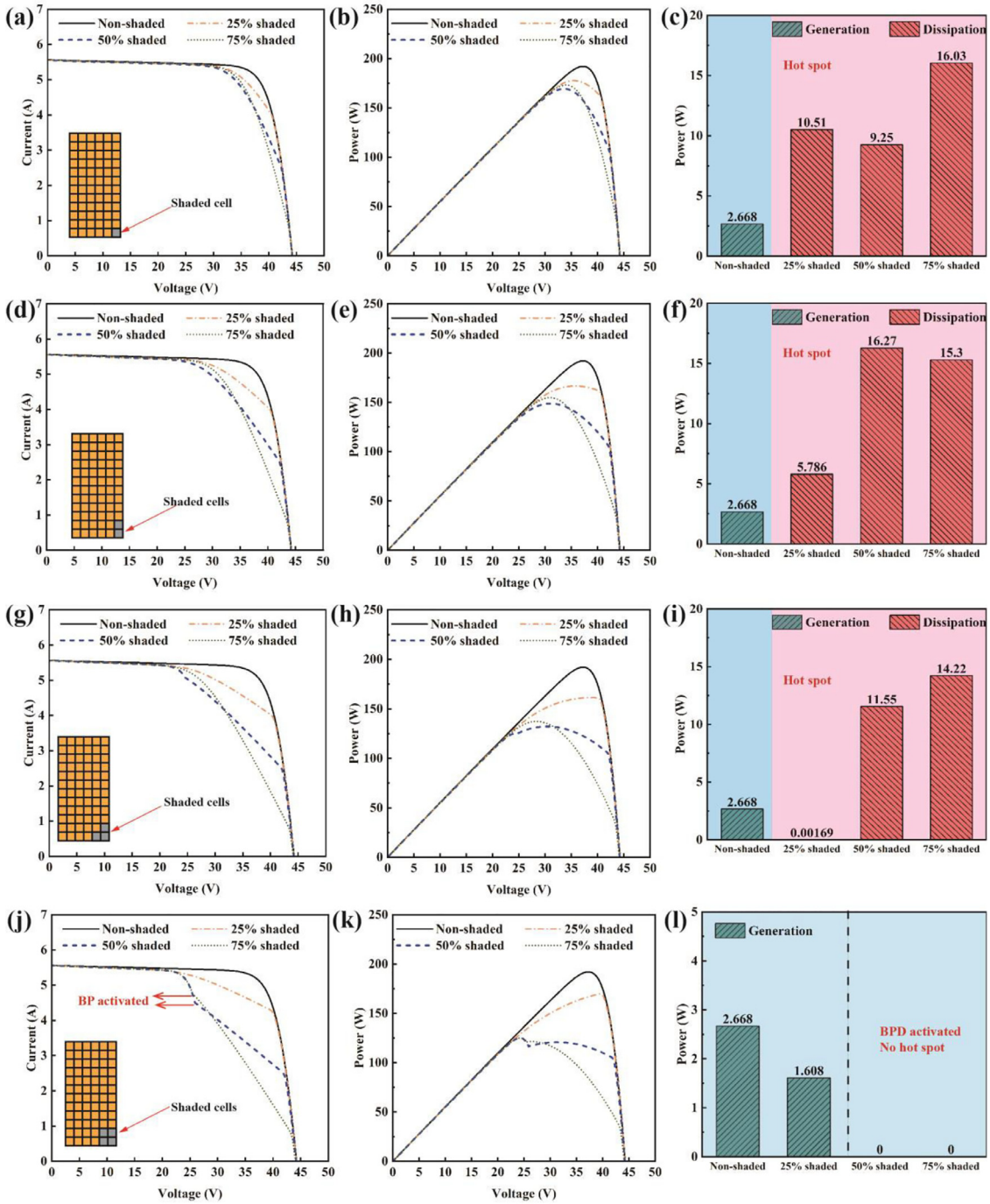


Fig. 12. Hot spot risk assessment of the module. (a–c) I-V curves, P-V curves, and hot spot assessment for pattern 1. (d–f) I-V curves, P-V curves, and hot spot assessment for pattern 2. (g–i) I-V curves, P-V curves, and hot spot assessment for pattern 3. (j–l) I-V curves, P-V curves, and hot spot assessment for pattern 4.

demonstrate this point, a hot spot risk assessment is conducted on the module used in Section 3.3. The detailed settings of the case study are shown in Table S4, basically covering the possible shading patterns on a small scale.

Fig. 12(a–c) shows the assessment result of the module with one cell shaded. As indicated, in the high voltage range, the I-V curves (Fig. 12(a)) exhibit a slanted straight-line feature and the slope becomes steeper as the shading degrees rise. As a result, P-V curves (Fig. 12(b)) witness decreasing MPPs and flatter trends in the high voltage range. When the module operates at MPPs, as indicated in Fig. 12(c), the shaded cell is reverse biased with more than 9 W power dissipation locally. For the scenario with 75% shaded, the localized dissipation even

reaches 16 W, nearly 8 times the amount of the power generation of an unshaded cell. If the shading pattern lasts for a long time, it is very likely to cause a severe hot spot.

Fig. 12(d–f) shows the assessment result of the module with two shaded cells. In general, the results share the same features as the above scenarios. However, the slanted straight-line feature in the I-V curve and decreasing MPPs are more prominent, thus leading to higher power loss. Notably, the localized dissipated power can be larger than 15 W when the shading factor is more than 50%, which implies that the hot spot area is larger.

Fig. 12(g–i) shows the assessment result of the module with three shaded cells. Similarly, the I-V curves exhibit slanted straight-line fea-

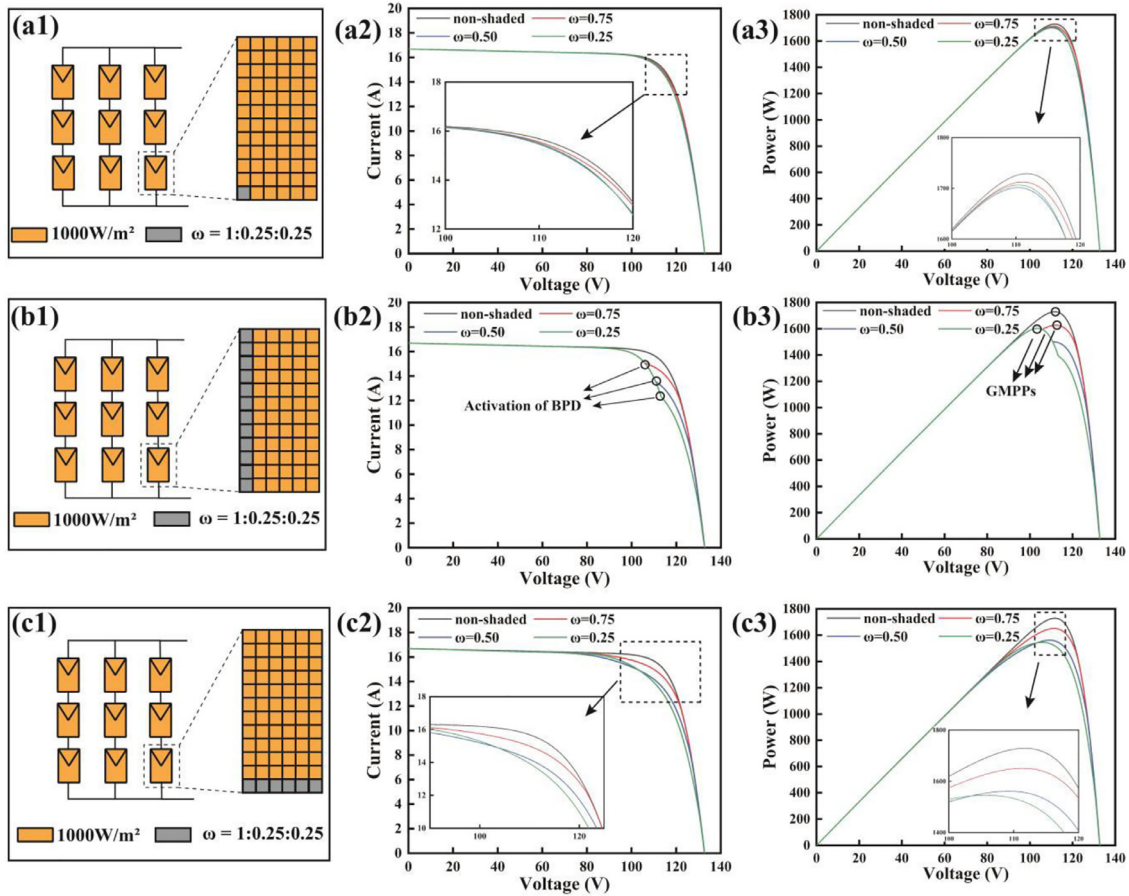


Fig. 13. The PSC settings and results of the high-resolution simulation. (a1-a3) single-cell PSC. (b1-b3) Longitudinal PSC. (c1-c3) Lateral PSC.

tures and the slope becomes steeper as the shading degrees rise. In Fig. 12(h), decreasing MPPs are also more prominent compared with the previous cases. When the module operates at MPPs, there is localized power dissipation in shaded cells as well. However, it can be noted that the power dissipation for 25% shaded is negligible, indicating that the current at MPP is very close to the short-circuit current of the shaded cell.

Fig. 12(j-l) shows the assessment result of the module with four shaded cells. As indicated in Fig. 12(j), despite that the straight-line features can be observed in the I-V curves with 50% and 75% shading degrees, this feature is quickly replaced by the ‘staircase shape’ when the voltage approaches 25 V. Correspondingly, the P-V curves exhibit two MPPs as indicated in Fig. 12(k). These changes are caused by the activation of the BPD connected in parallel with the CS. Since the protected CS will be bypassed when the BPD is activated, there is no power generated or dissipated in the shaded cells, thus avoiding the hot spot risks. However, it should be noted that if the MPP tracker fails, i.e., operating in the high voltage range, there are still hot spot risks.

Based on the above assessment, it can be concluded that there are high hot spot risks when the CS contains less than four shaded PV cells. The observed straight-line feature in I-V curves agrees with the experimental findings from the previous studies [28]. To mitigate or avoid this effect, the deployed site should avoid small-scale PSC, and regular cleaning to keep the surface clean is very important in operation. Simultaneously, the industry should select the PV cell carefully and find the optimal string length to develop a module less susceptible to hot spots. It is self-evident that the developed method can accelerate this R&D process.

4.2. Case 2: High-resolution simulation in array

The field measurement in the PV array has evidenced that even the PSC caused by the grass or the bird droppings can cause significant power loss [42]. Unfortunately, nearly all existing simulation programs neglect this effect which degrades the reliabilities of the simulation. The proposed method provides a ready way to address the issue. To demonstrate this point, three case studies are designed and conducted on the array used in Section 3.3, in which cell-level PSC is considered in the array-level simulation. Table S5 shows the settings of the shading scenarios and the following are the simulation results.

Fig. 13(a1-a3) shows the settings and the results of the array containing one shaded cell. As is shown in Fig. 13(a2), the current shrinks in the region near MPP as the shading degrees increase, leading the MPP to drop from 1729 W to 1696 W (Fig. 13(a3)). Simultaneously, this kind of PSC has a high risk of hot spots, which has been demonstrated in case 1. Thus, it is very important to keep the module surface clean and the deployed site open.

Fig. 13(b1-b3) shows the settings and the results when there is longitudinal PSC in the module. This kind of shading pattern can represent the PSC caused by the chimney and the shade from the nearby module. As is shown in Fig. 13(b2), due to the activation of the BPD, the I-V curve of the array shows a ‘staircase’ shape and the current of the second ‘step’ decreases as the shading degree increases. Correspondingly, there are two peaks in the P-V curve. The GMPP of the array drops from 1729 W to 1603 W as the shading degree increases (Fig. 13(b3)). However, if the MPPT is stuck in the LMPP, the output of the array is only 1393 W, and nearly 210 W is wasted.

Fig. 13(c1-c3) shows the settings and the results when there is lateral PSC in the module. As is shown in **Fig. 13(c2)**, the I-V curves share a similar feature to that of the single cell PSC but the phenomenon of current shrinking is more prominent. As a result, the MPP drops from 1729 W to 1546 W (**Fig. 13(c3)**). The cause of this significant loss is that there are more reverse-biased cells in the module.

Generally, the above case studies demonstrate the exclusive advantage of simulating the PV array in a high-resolution way. This merit allows an accurate prediction of power output, which provides a potential tool for research on the efficient array layout.

4.3. The novelties and limitations

4.3.1. The novelties

The proposed method provides an innovative way to model the electrical behaviors of PV systems (from a single solar cell to a large array) under general operating conditions (UIC or PSC). The consideration of the reverse-biased effect allows accurate and comprehensive characterization of the electrical behaviors at different levels. The bottom-up architecture enables the model to treat the electrical behavior and shading pattern diversity at the cell level. The efficient and robust numerical treatments improve the simulation efficiency without losing accuracy. Compared with the existing methods, this approach can estimate the electrical behaviors of the PV system operating in complex real-world scenarios. For performance prediction, this method not only possesses high accuracy and resolution but also includes some faults modeling ability. Common faults, including hot spots, current mismatch phenomena, or modules containing ill cells, can be easily modeled and analyzed. For large PV systems, the proposed method can serve as a simulation platform to assist the development and application of array reconfiguration and model-based MPPT algorithms.

4.3.2. The limitations

Inevitably, some limitations need to be considered. Firstly, the cell temperature is calculated coarsely using the NOCT method, which neglects the coupled effect between the heat transfer and power generation/dissipation. A detailed thermal model considering the hot spots effect should be introduced. Secondly, valid optical modeling is needed to obtain the shading matrix in complex surroundings handily. Then, the proposed method can compare different PV system topologies and select the optimal scheme, which can facilitate PV project planning. Thirdly, since there are many available reconfiguration or MPPT algorithms, the matched degrees between the developed method and them need further investigation. Lastly, rigorous validation against measurement is preferred at the array level to validate the effectiveness of the proposed method. These challenges are planned to be addressed in future studies.

5. Conclusions

An innovative and generalized method is presented to obtain the electrical behaviors of PV systems under complex PSC. An SSDM considering the reverse-biased behaviors is developed for a single solar cell and then stacked up to form the physics model of a module and array, respectively. A progressive validation process is designed and conducted to verify the effectiveness of the method. Two specially designed case studies are used to demonstrate the exclusive advantage of the proposed method. The main conclusions are drawn as follows:

- (1) The proposed method is valid for mainstream solar cell technologies (monocrystalline silicon, polycrystalline silicon, and thin film). The absolute error at MPP and the elapsed time are within 0.052 W and 0.01471 s, respectively.
- (2) Regardless of the PSC patterns on the module, the proposed method can characterize the electrical behavior properly. The maximum absolute error is within 3.45W while the elapsed time is within 0.015 s.

- (3) The proposed method achieves nearly identical results to Simulink when simulating the same array. But the proposed method contains more useful information and the elapsed time is nearly 20–50% less than that of Simulink.
- (4) Hot spot risk assessment in the PV module can be easily achieved via the proposed method. When the studied module is under small-scale PSC (less than 3 cells), the shaded cell can dissipate a considerable amount of power with a maximum of 16.27 W.
- (5) The proposed method can estimate the electrical behaviors of the large PV system in a fast and high-resolution way. This advantage can further facilitate the efficient PV system design in a specific condition.

In summary, the proposed method can simulate the PV system more realistically, especially for PV with complex PSC. As a fundamental and significant issue in PV research, it can be expected to play a significant role in many areas to advance the R&D of high-efficiency and long-lifespan systems. Future studies can focus on the detailed analysis of mismatch-induced fault and shading loss in large PV systems to propose mitigation measures. In addition, the optimal PV layout under complex building shadows can be an important topic to guide and facilitate PV project planning in urban scenarios. Lastly, the proposed framework also provides a solid basis for PV thermal management studies to combat hot spots and utilize waste heat.

Credit Author Statement

Fuxiang Li: Conceptualization, Methodology, Software, Data analysis, Writing- Original draft. **Wentao Dong:** Algorithm discussion, Coding suggestion. **Wei Wu:** Conceptualization, Methodology, Writing-reviewing and editing, Supervision, Funding acquisition.

Data availability

Data will be made available on request.

Acknowledgments

The authors gratefully acknowledge the support from the Research Grants Council of Hong Kong (Project number: [CityU 21201119](#), [CityU 11212620](#), [CityU 11215621](#), [CityU 11218922](#)).

Supplementary materials

Supplementary material associated with this article can be found, in the online version, at doi:[10.1016/j.adapen.2022.100118](https://doi.org/10.1016/j.adapen.2022.100118).

Appendix A. Ambient and parameter matrix in module

A.1. Ambient matrix

The expression of the shading matrix and temperature are:

$$\Omega^M = \begin{bmatrix} \omega(1, 1) & \dots & \omega(1, c) \\ \vdots & \ddots & \vdots \\ \omega(r, 1) & \dots & \omega(r, c) \end{bmatrix} \quad (A.1)$$

$$T^M = \begin{bmatrix} T^c(1, 1) & \dots & T^c(1, c) \\ \vdots & \ddots & \vdots \\ T^c(r, 1) & \dots & T^c(r, c) \end{bmatrix} \quad (A.2)$$

where superscript M denotes the module, r and c are the numbers of the rows and columns in the module. For example, $\omega(r, c)$ is the shading factor of the cell in the r^{th} row and c^{th} column.

A.2. Parameter matrix

$$\mathbf{I}_{ph}^M = \begin{bmatrix} I_{ph}^c(1, 1) & \dots & I_{ph}^c(1, c) \\ \vdots & \ddots & \vdots \\ I_{ph}^c(r, 1) & \dots & I_{ph}^c(r, c) \end{bmatrix} \quad (A.3)$$

$$\mathbf{I}_0^M = \begin{bmatrix} I_o^c(1, 1) & \dots & I_o^c(1, c) \\ \vdots & \ddots & \vdots \\ I_o^c(r, 1) & \dots & I_o^c(r, c) \end{bmatrix} \quad (A.4)$$

$$\mathbf{V}_t^M = \begin{bmatrix} V_t^c(1, 1) & \dots & V_t^c(1, c) \\ \vdots & \ddots & \vdots \\ V_t^c(r, 1) & \dots & V_t^c(r, c) \end{bmatrix} \quad (A.5)$$

$$\mathbf{R}_s^M = \begin{bmatrix} R_s^c(1, 1) & \dots & R_s^c(1, c) \\ \vdots & \ddots & \vdots \\ R_s^c(r, 1) & \dots & R_s^c(r, c) \end{bmatrix} \quad (A.6)$$

$$\mathbf{R}_p^M = \begin{bmatrix} R_p^c(1, 1) & \dots & R_p^c(1, c) \\ \vdots & \ddots & \vdots \\ R_p^c(r, 1) & \dots & R_p^c(r, c) \end{bmatrix} \quad (A.7)$$

where, \mathbf{I}_{ph}^M , \mathbf{I}_0^M , \mathbf{V}_t^M , \mathbf{R}_s^M and \mathbf{R}_p^M denote the parameter matrix of the five parameters, respectively.

Appendix B. Generalized ambient and parameter matrix in array

B.1. Generalized ambient matrix

For shadow information, the generalized ambient matrix Ω^A is expressed as follows:

$$\Omega^A = \begin{bmatrix} \Omega^M(1, 1) & \dots & \Omega^M(1, m) \\ \vdots & \ddots & \vdots \\ \Omega^M(n, 1) & \dots & \Omega^M(n, m) \end{bmatrix} \quad (B.1)$$

where Ω^A denotes the generalized shading matrix of the array, in which each element is a shading matrix. For example, $\Omega^M(n, 1)$ is the shading matrix in the n^{th} row and 1st column in the array.

Similarly, the temperature information can be organized as the generalized matrix T^A :

$$\mathbf{T}^A = \begin{bmatrix} \mathbf{T}^M(1, 1) & \dots & \mathbf{T}^M(1, m) \\ \vdots & \ddots & \vdots \\ \mathbf{T}^M(n, 1) & \dots & \mathbf{T}^M(n, m) \end{bmatrix} \quad (B.2)$$

B.2. Generalized ambient matrix

$$\mathbf{I}_{ph}^A = \begin{bmatrix} \mathbf{I}_{ph}^M(1, 1) & \dots & \mathbf{I}_{ph}^M(1, m) \\ \vdots & \ddots & \vdots \\ \mathbf{I}_{ph}^M(n, 1) & \dots & \mathbf{I}_{ph}^M(n, m) \end{bmatrix} \quad (B.3)$$

$$\mathbf{I}_0^A = \begin{bmatrix} \mathbf{I}_0^M(1, 1) & \dots & \mathbf{I}_0^M(1, m) \\ \vdots & \ddots & \vdots \\ \mathbf{I}_0^M(n, 1) & \dots & \mathbf{I}_0^M(n, m) \end{bmatrix} \quad (B.4)$$

$$\mathbf{V}_t^A = \begin{bmatrix} \mathbf{V}_t^M(1, 1) & \dots & \mathbf{V}_t^M(1, m) \\ \vdots & \ddots & \vdots \\ \mathbf{V}_t^M(n, 1) & \dots & \mathbf{V}_t^M(n, m) \end{bmatrix} \quad (B.5)$$

$$\mathbf{R}_s^A = \begin{bmatrix} \mathbf{R}_s^M(1, 1) & \dots & \mathbf{R}_s^M(1, m) \\ \vdots & \ddots & \vdots \\ \mathbf{R}_s^M(n, 1) & \dots & \mathbf{R}_s^M(n, m) \end{bmatrix} \quad (B.6)$$

$$\mathbf{R}_p^A = \begin{bmatrix} \mathbf{R}_p^M(1, 1) & \dots & \mathbf{R}_p^M(1, m) \\ \vdots & \ddots & \vdots \\ \mathbf{R}_p^M(n, 1) & \dots & \mathbf{R}_p^M(n, m) \end{bmatrix} \quad (B.7)$$

where \mathbf{I}_{ph}^A , \mathbf{I}_0^A , \mathbf{V}_t^A , \mathbf{R}_s^A and \mathbf{R}_p^A denote the generalized parameter matrix of the five parameters, respectively.

References

- [1] Wang K, Yang D, Wu C, Shapter J, Priya S. Mono-crystalline Perovskite Photovoltaics toward Ultrahigh Efficiency? Joule 2019;3:311–16. doi:[10.1016/j.joule.2018.11.009](https://doi.org/10.1016/j.joule.2018.11.009).
- [2] Mei J, Zuo Y, Lee CHT, Wang X, Kirtley JL. Stochastic optimization of multi-energy system operation considering hydrogen-based vehicle applications. Adv Appl Energy 2021;2:100031. doi:[10.1016/j.adapen.2021.100031](https://doi.org/10.1016/j.adapen.2021.100031).
- [3] Huen P, Daoud WA. Advances in hybrid solar photovoltaic and thermoelectric generators. Renew Sustain Energy Rev 2017;72:1295–302. doi:[10.1016/j.rser.2016.10.042](https://doi.org/10.1016/j.rser.2016.10.042).
- [4] Yu G, Yang H, Lu D, Cheng X, Ansah MK. A review on developments and researches of building integrated photovoltaic (BIPV) windows and shading blinds. Renew Sustain Energy Rev 2021;149. doi:[10.1016/j.rser.2021.111355](https://doi.org/10.1016/j.rser.2021.111355).
- [5] Wei M, Lee SH, Hong T, Conlon B, McKenzie L, Hendron B, et al. Approaches to cost-effective near-net zero energy new homes with time-of-use value of energy and battery storage. Adv Appl Energy 2021;2:100018. doi:[10.1016/j.adapen.2021.100018](https://doi.org/10.1016/j.adapen.2021.100018).
- [6] Mittelviehfaus M, Georges G, Boulochos K. Electrification of multi-energy hubs under limited electricity supply: De-/centralized investment and operation for cost-effective greenhouse gas mitigation. Adv Appl Energy 2022;5:100083. doi:[10.1016/j.adapen.2022.100083](https://doi.org/10.1016/j.adapen.2022.100083).
- [7] Marqusee J, Becker W, Ericson S. Resilience and economics of microgrids with PV, battery storage, and networked diesel generators. Adv Appl Energy 2021;3:100049. doi:[10.1016/j.adapen.2021.100049](https://doi.org/10.1016/j.adapen.2021.100049).
- [8] Sabadini F, Madlener R. The economic potential of grid defection of energy prosumer households in Germany. Adv Appl Energy 2021;4:100075. doi:[10.1016/j.adapen.2021.100075](https://doi.org/10.1016/j.adapen.2021.100075).
- [9] Tsanakas JA, Ha L, Buerhop C. Faults and infrared thermographic diagnosis in operating c-Si photovoltaic modules: a review of research and future challenges. Renew Sustain Energy Rev 2016;62:695–709. doi:[10.1016/j.rser.2016.04.079](https://doi.org/10.1016/j.rser.2016.04.079).
- [10] Ma T, Yang H, Lu L. Long term performance analysis of a standalone photovoltaic system under real conditions. Appl Energy 2017;201:320–31. doi:[10.1016/j.apenergy.2016.08.126](https://doi.org/10.1016/j.apenergy.2016.08.126).
- [11] Fertig F, Willibald C, Geisemeyer I, Schubert MC, Rein S. Illumination and temperature dependence of breakdown mechanisms in multi-crystalline silicon solar cells. Energy Procedia 2013;38:32–42. doi:[10.1016/j.egypro.2013.07.246](https://doi.org/10.1016/j.egypro.2013.07.246).
- [12] Yang B, Yu T, Zhang X, Li H, Shu H, Sang Y, et al. Dynamic leader based collective intelligence for maximum power point tracking of PV systems affected by partial shading condition. Energy Convers Manag 2019;179:286–303. doi:[10.1016/j.enconman.2018.10.074](https://doi.org/10.1016/j.enconman.2018.10.074).
- [13] Galeano AG, Bressan M, Vargas FJ, Alonso C. Shading ratio impact on photovoltaic modules and correlation with shading patterns. Energies 2018;11. doi:[10.3390/en11040852](https://doi.org/10.3390/en11040852).
- [14] Yang B, Zhong L, Zhang X, Shu H, Yu T, Li H, et al. Novel bio-inspired memetic salp swarm algorithm and application to MPPT for PV systems considering partial shading condition. J Clean Prod 2019;215:1203–22. doi:[10.1016/j.jclepro.2019.01.150](https://doi.org/10.1016/j.jclepro.2019.01.150).
- [15] Ram JP, Manghani H, Pillai DS, Babu TS, Miyatake M, Rajasekar N. Analysis on solar PV emulators: a review. Renew Sustain Energy Rev 2018;81:149–60. doi:[10.1016/J.RSER.2017.07.039](https://doi.org/10.1016/J.RSER.2017.07.039).
- [16] Ma T, Gu W, Shen L, Li M. An improved and comprehensive mathematical model for solar photovoltaic modules under real operating conditions. Sol Energy 2019;184:292–304. doi:[10.1016/J.SOLENER.2019.03.089](https://doi.org/10.1016/J.SOLENER.2019.03.089).
- [17] Ishaque K, Salam Z, Taheri H. Simple, fast and accurate two-diode model for photovoltaic modules. Sol Energy Mater Sol Cells 2011;95:586–94. doi:[10.1016/j.solmat.2010.09.023](https://doi.org/10.1016/j.solmat.2010.09.023).
- [18] Soon JJ, Low KS, Goh ST. Multi-dimension diode photovoltaic (PV) model for different PV cell technologies. IEEE Int Symp Ind Electron 2014;2496–501. doi:[10.1109/ISIE.2014.6865012](https://doi.org/10.1109/ISIE.2014.6865012).
- [19] Kermadi M, Chin VJ, Mekhilef S, Salam Z. A fast and accurate generalized analytical approach for PV arrays modeling under partial shading conditions. Sol Energy 2020;208:753–65. doi:[10.1016/J.SOLENER.2020.07.077](https://doi.org/10.1016/J.SOLENER.2020.07.077).
- [20] Bai J, Liu S, Hao Y, Zhang Z, Jiang M, Zhang Y. Development of a new compound method to extract the five parameters of PV modules. Energy Convers Manag 2014;79:294–303. doi:[10.1016/j.enconman.2013.12.041](https://doi.org/10.1016/j.enconman.2013.12.041).
- [21] Zhu L, Li Q, Chen M, Cao K, Sun Y. A simplified mathematical model for power output predicting of Building Integrated Photovoltaic under partial shading conditions. Energy Convers Manag 2019;180:831–43. doi:[10.1016/J.ENCONMAN.2018.11.036](https://doi.org/10.1016/J.ENCONMAN.2018.11.036).
- [22] Ma J, Hong D, Wang K, Bi Z, Zhu X, Zhang J. Analytical modeling and parameter estimation of photovoltaic strings under partial shading conditions. Sol Energy Mater Sol Cells 2022;235:111494. doi:[10.1016/J.SOLMAT.2021.111494](https://doi.org/10.1016/J.SOLMAT.2021.111494).
- [23] Wu J, Zhang L, Liu Z, Luo Y, Wu Z, Wang Z, Zhang J. Experimental and theoretical study on semi-transparent photovoltaic glazing façade under shaded conditions. Energy 2020;207:118314. doi:[10.1016/j.energy.2020.118314](https://doi.org/10.1016/j.energy.2020.118314).
- [24] Guerriero P, Tricoli P, Daliento S. A bypass circuit for avoiding the hot spot in PV modules. Sol Energy 2019;181:430–8. doi:[10.1016/j.solener.2019.02.010](https://doi.org/10.1016/j.solener.2019.02.010).

- [25] Bishop JW. Computer simulation of the effects of electrical mismatches in photovoltaic cell interconnection circuits. *Sol Cells* 1988;25:73–89. doi:[10.1016/0379-6787\(88\)90059-2](https://doi.org/10.1016/0379-6787(88)90059-2).
- [26] Orozco-Gutierrez ML, Ramirez-Scarpetta JM, Spagnuolo G, Ramos-Paja CA. A method for simulating large PV arrays that include reverse biased cells. *Appl Energy* 2014;123:157–67. doi:[10.1016/j.apenergy.2014.02.052](https://doi.org/10.1016/j.apenergy.2014.02.052).
- [27] Zhang Y, Su J, Zhang C, Lang Z, Yang M, Gu T. Performance estimation of photovoltaic module under partial shading based on explicit analytical model. *Sol Energy* 2021;224:327–40. doi:[10.1016/J.SOLENER.2021.06.019](https://doi.org/10.1016/J.SOLENER.2021.06.019).
- [28] Zhang Z, Ma M, Wang H, Wang H, Ma W, Zhang X. A fault diagnosis method for photovoltaic module current mismatch based on numerical analysis and statistics. *Sol Energy* 2021;225:221–36. doi:[10.1016/j.solener.2021.07.037](https://doi.org/10.1016/j.solener.2021.07.037).
- [29] Kim KA, Krein PT. Photovoltaic hot spot analysis for cells with various reverse-bias characteristics through electrical and thermal simulation. In: Proceedings of the IEEE 14th Work Control Model Power Electron COMPEL 2013; 2013.
- [30] Waqar Akram M, Li G, Jin Y, Zhu C, Javaid A, Zuhai Akram M, et al. Study of manufacturing and hotspot formation in cut cell and full cell PV modules. *Sol Energy* 2020;203:247–59. doi:[10.1016/J.SOLENER.2020.04.052](https://doi.org/10.1016/J.SOLENER.2020.04.052).
- [31] Clement CE, Singh JP, Khoo YS, Halm A, Tune D, Birgersson E. Design of shading- and hotspot-resistant shingled modules. *Prog Photovolt Res Appl* 2022;30:464–80. doi:[10.1002/pip.3507](https://doi.org/10.1002/pip.3507).
- [32] Klasen N, Weisser D, Rößler T, Neuhaus DH, Kraft A. Performance of shingled solar modules under partial shading. *Prog Photovolt Res Appl* 2022;30:325–38. doi:[10.1002/pip.3486](https://doi.org/10.1002/pip.3486).
- [33] Mehedri IM, Salam Z, Ramli MZ, Chin VJ, Bassi H, Rawi MJH, et al. Critical evaluation and review of partial shading mitigation methods for grid-connected PV system using hardware solutions: the module-level and array-level approaches. *Renew Sustain Energy Rev* 2021;146:111138. doi:[10.1016/j.rser.2021.111138](https://doi.org/10.1016/j.rser.2021.111138).
- [34] Yang B, Shao R, Zhang M, Ye H, Liu B, Bao T, et al. Socio-inspired democratic political algorithm for optimal PV array reconfiguration to mitigate partial shading. *Sustain Energy Technol Assess* 2021;48:101627. doi:[10.1016/j.seta.2021.101627](https://doi.org/10.1016/j.seta.2021.101627).
- [35] Yang B, Yu T, Shu H, Dong J, Jiang L. Robust sliding-mode control of wind energy conversion systems for optimal power extraction via nonlinear perturbation observers. *Appl Energy* 2018;210:711–23. doi:[10.1016/j.apenergy.2017.08.027](https://doi.org/10.1016/j.apenergy.2017.08.027).
- [36] Yang B, Wang J, Zhang X, Yu T, Yao W, Shu H, et al. Comprehensive overview of meta-heuristic algorithm applications on PV cell parameter identification. *Energy Convers Manag* 2020;208:112595. doi:[10.1016/J.ENCONMAN.2020.112595](https://doi.org/10.1016/J.ENCONMAN.2020.112595).
- [37] Yang B, Ye H, Wang J, Li J, Wu S, Li Y, et al. PV arrays reconfiguration for partial shading mitigation: recent advances, challenges and perspectives. *Energy Convers Manag* 2021;247:114738. doi:[10.1016/j.enconman.2021.114738](https://doi.org/10.1016/j.enconman.2021.114738).
- [38] Yang B, Zhu T, Wang J, Shu H, Yu T, Zhang X, et al. Comprehensive overview of maximum power point tracking algorithms of PV systems under partial shading condition. *J Clean Prod* 2020;268:121983. doi:[10.1016/j.jclepro.2020.121983](https://doi.org/10.1016/j.jclepro.2020.121983).
- [39] Li P, Zhang H, Guo Z, Lyu S, Chen J, Li W, et al. Understanding rooftop PV panel semantic segmentation of satellite and aerial images for better using machine learning. *Adv Appl Energy* 2021;4:100057. doi:[10.1016/j.adapen.2021.100057](https://doi.org/10.1016/j.adapen.2021.100057).
- [40] Walker L, Hofer J, Schlueter A. High-resolution, parametric BIPV and electrical systems modeling and design. *Appl Energy* 2019;238:164–79. doi:[10.1016/j.apenergy.2018.12.088](https://doi.org/10.1016/j.apenergy.2018.12.088).
- [41] Chen X, Du Y, Lim E, Wen H, Yan K, Kirtley J. Power ramp-rates of utility-scale PV systems under passing clouds: module-level emulation with cloud shadow modeling. *Appl Energy* 2020;268:114980. doi:[10.1016/j.apenergy.2020.114980](https://doi.org/10.1016/j.apenergy.2020.114980).
- [42] Ilse K, Micheli L, Figgis BW, Lange K, Dafslér D, Hanifi H, et al. Techno-economic assessment of soiling losses and mitigation strategies for solar power generation. *Joule* 2019;3:2303–21. doi:[10.1016/J.JOULE.2019.08.019](https://doi.org/10.1016/J.JOULE.2019.08.019).
- [43] Laarabi B, Sankarkumar S, Rajasekar N, El Baqqal Y, Barhdadi A. Modeling investigation of soiling effect on solar photovoltaic systems: new findings. *Sustain Energy Technol Assess* 2022;52:102126. doi:[10.1016/J.SETA.2022.102126](https://doi.org/10.1016/J.SETA.2022.102126).
- [44] Diaz-Dorado E, Cidras J, Carrillo C. Discrete I-V model for partially shaded PV-arrays. *Sol Energy* 2014;103:96–107. doi:[10.1016/j.solener.2014.01.037](https://doi.org/10.1016/j.solener.2014.01.037).
- [45] Li F, Wu W. Coupled electrical-thermal performance estimation of photovoltaic devices: a transient multiphysics framework with robust parameter extraction and 3-D thermal analysis. *Appl Energy* 2022;319:119249. doi:[10.1016/J.APENERGY.2022.119249](https://doi.org/10.1016/J.APENERGY.2022.119249).
- [46] Simulink. PV array simulation [Online]. Available: <https://www.mathworks.cn/help/sps/powersys/ref/pvarray.html> [accessed 14/7/2022].
- [47] PV Syst SA. PVSYST- Photovoltaic Software [Online]. Available: <https://www.pvsyst.com/> [accessed 14/7/2022].
- [48] Liu G, Nguang SK, Partridge A. A general modeling method for I-V characteristics of geometrically and electrically configured photovoltaic arrays. *Energy Convers Manag* 2011;52:3439–45. doi:[10.1016/j.enconman.2011.07.011](https://doi.org/10.1016/j.enconman.2011.07.011).
- [49] Mekki H, Mellit A, Salhi H. Artificial neural network-based modelling and fault detection of partial shaded photovoltaic modules. *Simul Model Pract Theory* 2016;67:1–13. doi:[10.1016/j.simpat.2016.05.005](https://doi.org/10.1016/j.simpat.2016.05.005).
- [50] Kanwal S, Khan B, Ali SM, Mehrnoor CA, Rauf MQ. Support vector machine and Gaussian process regression based modeling for photovoltaic power prediction. In: Proceedings of the 2018 International Conference on Frontiers of Information Technology (FIT); 2019. p. 117–22. doi:[10.1109/FIT.2018.00028](https://doi.org/10.1109/FIT.2018.00028).
- [51] Ma T, Gu W, Shen L, Li M. An improved and comprehensive mathematical model for solar photovoltaic modules under real operating conditions. *Sol Energy* 2019;184:292–304. doi:[10.1016/j.solener.2019.03.089](https://doi.org/10.1016/j.solener.2019.03.089).
- [52] Wang J, Yang B, Li D, Zeng C, Chen Y, Guo Z, et al. Photovoltaic cell parameter estimation based on improved equilibrium optimizer algorithm. *Energy Convers Manag* 2021;236:114051. doi:[10.1016/j.enconman.2021.114051](https://doi.org/10.1016/j.enconman.2021.114051).
- [53] Villalva MG, Gazoli JR, Filho ER. Comprehensive approach to modeling and simulation of photovoltaic arrays. *IEEE Trans Power Electron* 2009;24:1198–208. doi:[10.1109/TPEL.2009.2013862](https://doi.org/10.1109/TPEL.2009.2013862).
- [54] Restrepo-Cuestas BJ, Montano J, Ramos-Paja CA, Trejos-Grisales LA, Orozco-Gutierrez ML. Parameter estimation of the bishop photovoltaic model using a genetic algorithm. *Appl Sci* 2022;12. doi:[10.3390/app12062927](https://doi.org/10.3390/app12062927).
- [55] Berardi U, Graham J. Investigation of the impacts of microclimate on PV energy efficiency and outdoor thermal comfort. *Sustain Cities Soc* 2020;62:102402. doi:[10.1016/J.SCS.2020.102402](https://doi.org/10.1016/J.SCS.2020.102402).
- [56] Boccalatte A, Fossa M, Ménézo C. Best arrangement of BIPV surfaces for future NZEB districts while considering urban heat island effects and the reduction of reflected radiation from solar façades. *Renew Energy* 2020;160:686–97. doi:[10.1016/j.renene.2020.07.057](https://doi.org/10.1016/j.renene.2020.07.057).